

Zircon U–Pb geochronology and Sr–Nd isotopes of volcanic rocks from the Dahalajunshan Formation: implications for Late Devonian–Middle Carboniferous tectonic evolution of the Chinese Western Tianshan

Xinqi Yu¹ · Zongxiu Wang² · Xiang Zhou³ · Weifeng Xiao² · Xinpeng Yang¹

Received: 20 August 2014 / Accepted: 12 November 2015 / Published online: 15 December 2015
© Springer-Verlag Berlin Heidelberg 2015

Abstract The widespread Late Devonian–Middle Carboniferous volcanic rocks in the Chinese Western Tianshan provide important constraints on the subduction history of the South Tianshan oceanic lithosphere. Here, we investigate the basalt, basaltic andesite, andesite, trachyandesite, and rhyolite from the Dahalajunshan Formation from Western Tianshan. Laser ablation inductively coupled plasma mass spectrometry (LA–ICP–MS) U–Pb zircon geochronology constrains their age of formation to between 376 and 333 Ma (i.e., Late Devonian–Middle Carboniferous) with distinct variation in space (from west to east) and time (from early to late). Based on geochemical, zircon geochronological, and Sr–Nd isotopic data, we demonstrate that the Dahalajunshan volcanic was generated in a continental arc setting associated with the subduction of the south Tianshan Ocean during Late Devonian to Middle Carboniferous. The volcanic rocks belonging to Dahalajunshan Formation in the northwestern part of the Yili Block suggest that the northward subduction of the south Tianshan Ocean was initiated in the Early Devonian; those in the southern and eastern part of the Yili Block were probably produced by a northward subduction of South Tianshan Ocean during Late Devonian to Middle Carboniferous.

Keywords Dahalajunshan Formation · Late Devonian–Middle Carboniferous · LA–ICP–MS · Sr–Nd isotope · Western Tianshan

Introduction

Late Paleozoic volcanic rocks are widespread in the Chinese Western Tianshan and are considered to have formed during the subduction of Southern Tianshan Oceanic Basin (Jiang et al. 1993; Wu et al. 1995; Gao et al. 1997; Ma et al. 2007; Li et al. 2009a, b; Zhu et al. 2006a, b, 2010, 2011, 2012). Although previous studies provided evidence supporting this hypothesis, controversies still remain. These disputes focus on the temporal and spatial regularity of volcanic activity and on the tectonic setting of Late Paleozoic volcanic rocks in Yining, Tekes, and Nalati areas within and/or surrounding the Yili Block. In particular, the dispute focuses on the age of formation and tectonic environment of the Dahalajunshan volcanic rocks, which constitute an important ore-bearing strata in West Tianshan (Xiao et al. 2005; Zhu et al. 2006a; Luo et al. 2009; Yang et al. 2009; Zhai et al. 2009; Li et al. 2012b; Ru et al. 2012).

The geochronological data reported in earlier studies have led to controversy regarding tectono-magmatic events in the West Tianshan arc complex. Previous workers believed that the age range of formation of the Dahalajunshan Formation from west to east of the Yili Block is 358–310 Ma (Zhu et al. 2005b; Zhang et al. 2009; Ru et al. 2012) during Carboniferous period. Several recent investigations have presented new age data from this region. Li et al. (2012a) conducted LA–ICP–MS of U–Pb zircon analyses on two rhyolites along the northern boundary of the Yili block and obtained ages between 369.7 ± 4.9 and 363.4 ± 2.5 Ma. Zhai et al. (2006) performed sensitive

✉ Xinqi Yu
yuxinqi@cugb.edu.cn

¹ School of the Earth Sciences and Resources, China University of Geosciences, Beijing 100083, China

² Institute of Geomechanics, Chinese Academy of Geological Sciences, Beijing 100081, China

³ Faculty of Earth Sciences, China University of Geosciences, Wuhan 430074, China

high-resolution ion microprobe (SHRIMP) of U–Pb zircon and reported an age of 363 Ma from the quartz andesite occurring as host rock in the Axi gold deposit. Zhu et al. (2006a) reported SHRIMP zircon age of basaltic andesite as 363.1 Ma. Zhu et al. (2009) further showed that the SHRIMP zircon age of andesite from Tekes area is 361 Ma. Thus, volcanic rocks of Dahalajunshan Formation in Western Tianshan area can be divided into three age groups around the Yili Block, namely Late Devonian in the west, Early Carboniferous in the central, and Late Carboniferous in the east. Some intermediate ages have also been reported. However, the volcanic rocks that belong to different stages were considered as discrete units and could not be grouped commonly under the Dahalajunshan Formation (Zhai et al. 2006; Zhu et al. 2006a, 2009; Li et al. 2012a; An et al. 2013). On the basis of the Late Devonian zircon ages of 369.7 ± 4.9 and 363.4 ± 2.5 Ma from rhyolites, Li et al. (2012a) considered that these volcanic rocks belonging to Late Devonian should be distinguished from the previously defined Dahalajunshan Formation of Early Carboniferous and suggested a new classification as Upper Devonian “Yuzan Formation.”

Among the various proposals for the tectonic setting of the volcanic rocks in the Dahalajunshan Formation, three models remain controversial. The first one proposes that the volcanic rocks might have been formed in a continental rift setting in post-orogenic extensional stage (Che et al. 1996; Xia et al. 2006, 2008, 2012; Li et al. 2012b). The second model considers that these rocks might have formed in an island arc or continental marginal arc, associated with the subduction of Southern Tianshan Oceanic Basin under the Yili–Middle Tianshan Plate (Zhu et al. 2005a; Zhang and Li 2006; Ma et al. 2007; Long et al. 2008; Xia et al. 2011). The third model proposes that these volcanic rocks formed during extension in a typical volcanic arc setting, and is different from a continental rift environment (Qian et al. 2006). The debates surrounding the origin of these rocks are mainly due to the lack of precise information on the composition, structure, and timing of the episodic eruptions of the Dahalajunshan Formation volcanic rocks.

Because the volcanic rocks of Dahalajunshan Formation recorded the important information of the subduction of the South Tianshan Ocean in Late Paleozoic in Western Tianshan, in this study, we applied LA–ICP–MS zircon U–Pb geochronology and Sr–Nd isotopic analyses to understand the spatial–temporal distributions of the Dahalajunshan volcanic rocks and their originated sources. Combined with the results from previous studies, we evaluate the tectonic significance and its implications on the development of Tianshan Orogen and associated ocean-continent transition process. It is expected that our comprehensive study on the Dahalajunshan volcanic rocks should help placing more

constraints on the kinematics and age of orogenic process of the Central Asian Orogenic Belt.

Lithological characteristics

The available geological data indicate that Devonian and Carboniferous volcanic rocks are widely distributed in Chinese West Tianshan where they range in thickness of over 3000 m in most cases and sometimes >10,000 m (Bureau of Geology and Mineral Resources of Xinjiang Uygur Autonomous Region, 1993, 1999). Among these thick volcanic rocks, the Dahalajunshan Formation contains a set of amaranth-grayish-green intermediate-acid lava, volcanoclastic rocks, sandstones, and conglomerates with a few limestones (Bureau of Geology and Mineral Resources of Xinjiang Uygur Autonomous Region, 1993, 1999). The thickest layer appears in the Yili basin (Yining area) with a thickness of 4543.5 m (Bureau of Geology and Mineral Resources of Xinjiang Uygur Autonomous Region, 1993). The term “Dahalajunshan Formation” was extensively used to refer to a combination of volcanic–sedimentary rocks composed of a lower layer of basalt, trachyte, trachyandesite tuff, and volcanic breccia, as well as an upper layer of rhyolite, trachyte, tuff (with sandstone), and limestone lens (Shao et al. 2006; Liu 2007; Li et al. 2008). These rocks are widely distributed around the Yili Block (Fig. 1). The easternmost portion of the formation appears in the east of Nalati, whereas the westernmost portion, as a previously delineated through 1:200,000-scale geological mapping, lies along the boundary between China and Kazakhstan. This location is in the upper reaches of Lucaogou River (west of Sayram Lake, significantly higher than the Mazigou Village), Yining City. Our observation indicates that the bottom of volcanic gravel layer unconformably overlies the Ordovician limestone of Hudukedaban Formation (Fig. 2).

According to the profiles examined along the observation route (Fig. 1), marked variations are observed in the lithology of the Dahalajunshan Formation from west to east of the Chinese West Tianshan. This observation is similar to those described in previous segmental studies. In the westernmost spot TS35-2 (Fig. 2c) and the northeast of western Yining TS31-2 (Fig. 3a), brecciated andesitic basalts composed of giant exposures of breccia with purple andesitic cement are found. The gravel is primarily andesite with minor amounts of siliceous rocks and locally sandstone gravel. The gravel is also large and round but poorly sorted (Fig. 3b). Particles are thinner with a weaker alignment dipping toward 180° with a dip angle of 40° . The surrounding rock of the Axi gold deposit (TS26-1) consists of continental volcanic rocks. Typical volcanic mud ball structures caused by pyroclastic flows on continental facies can also

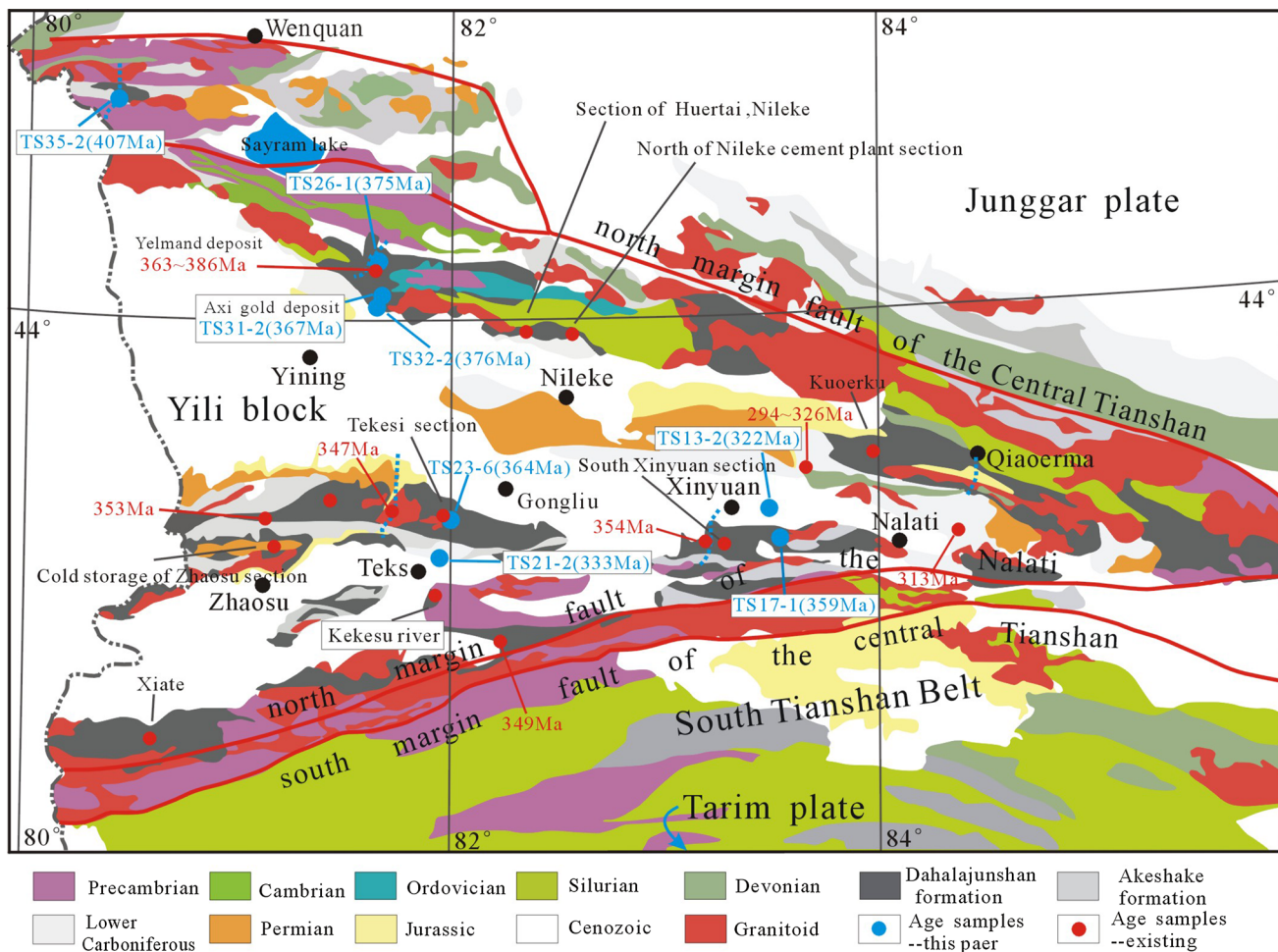


Fig. 1 Distribution diagram of the Dahalajunshan Formation (revised after Gao et al. 2009)

be observed in ignimbrite and rhyolitic lava tuff breccia of Zhaosu area. Approximately demarcated by 82° west longitude, a series of shallow marine to continental facies of volcanic rocks, such as effusive, explosive, minor eruption-sedimentary, subvolcanic, and volcanic channel facies, can also be identified. To the east, marine features of the interlayer of marine limestone, fluid (Fig. 3c), and bulb structures were observed. Zhang (2012) discovered evidence of abundant fossils at the bottom of the Nileke profile and noted two layers of volcanic molten balls in volcanic rocks below a marine limestone layer; this evidence indicates that the formation gradually transitioned from a continental eruption into a marine facies. The majority of Dahalajunshan Formation in Xinyuan and Tekes areas is a group of intermediate-basic volcanic rocks (porphyry; Fig. 3d) which show transition to intermediate-felsic marine volcanic rocks.

Broadly two belts of Dahalajunshan volcanic rocks are distributed in west Chinese Tianshan. The northern

one appears in the north-northwest within Yili Block and mainly includes andesites, brecciated andesitic basalts, etc., whereas the other one occurs in the southern margin, east of Yili Block, and contains basalt, andesite, rhyolite, and tuff.

Analytical methods

In this study, we investigated all the rock types in the Dahalajunshan Formation around Yili Block, such as southern Xinyuan County, Nalati area, Turks area, Zhaosu area, and Axi gold deposit. Representative samples were collected along the sections (Fig. 1) for geochemical analyses (26 samples) and LA-ICP-MS zircon U-Pb dating (11 samples), as well as Sm, Nd, Rb, and Sr measurements (23 samples), with a view to understand the formation mechanism, timing, and tectonic significance.

Fig. 2 Characteristics of the Dahalajunshan Formation rocks in the upper reaches of Lucaogou river (west of Sayram Lake, much higher than the Mazigou village), Yining City

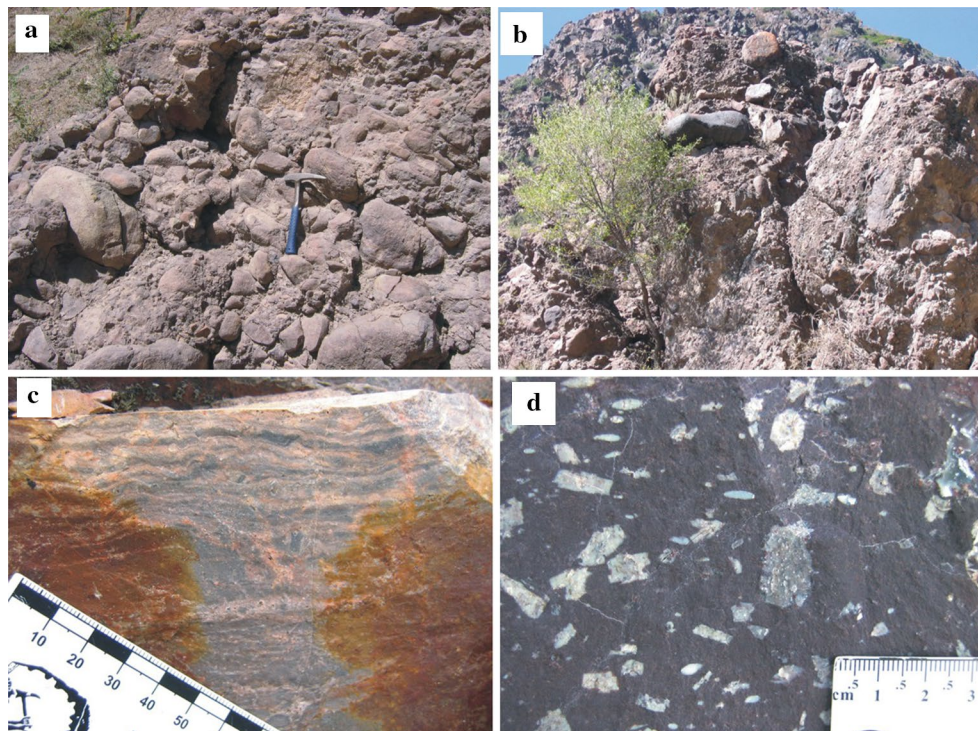
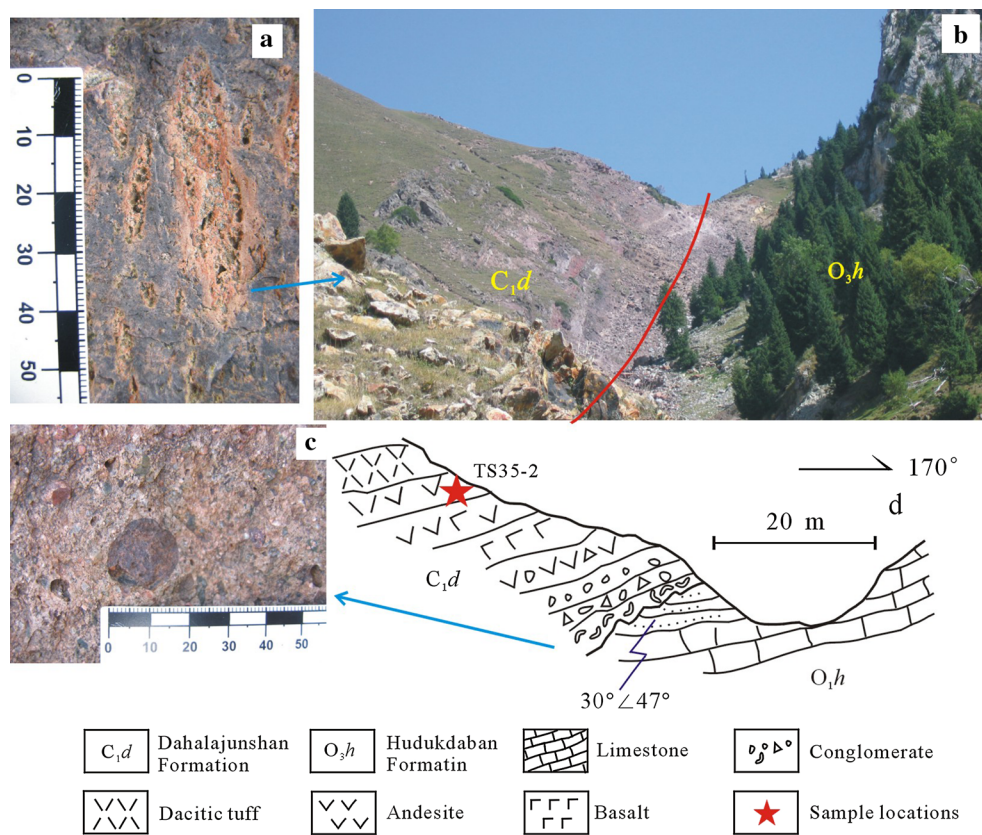


Fig. 3 Characteristics of Dahalajunshan Formation rock outcrops: **a** andesitic basal conglomerate in the upper reaches of the river in northern Yining County, **b** andesitic, sandstone, and large well-

rounded but poorly sorted gravel in the upper reaches of the river in northern Yining County, **c** rhyolite in northern Tekes, and **d** andesitic porphyry in southern Xinyuan

Bulk-rock geochemical analyses

Bulk-rock samples were collected from each section (Fig. 1) for geochemical analysis. The sample details and rock types are listed in Table 1.

Bulk-rock geochemical analyses were conducted by ALS Chemex of Guangzhou. Rock samples with fresh and non-weathered faces were selected. The bulk-rock samples were crushed into <1 cm fragments and soaked in HCl solution for 2–3 h. The fragments were then washed with distilled water. The fragments were completely dried and then crushed to <200 mesh by using a pollution-free agate ball mill before elemental contents were determined.

These powdered samples were calcined, and $\text{Li}_2\text{B}_4\text{O}_7$ – LiBO_2 was added and thoroughly mixed; afterward, the samples were placed in an automatic melting apparatus at >1000 °C. A melted sample was poured to form a flat sheet of glass, and an X-ray fluorescence spectrometer was used for analysis to determine the major elements. For rare earth element (REE) content, nitric acid was used to prepare the solution, which was then analyzed by plasma mass spectrometry (ICP–MS). We performed plasma emission spectroscopy instrumentation (ICP–AES) and ICP–MS to determine trace elements. The samples digested with perchloric acid, nitric acid, and hydrofluoric acid were dissolved with dilute hydrochloric acid to a constant volume for analysis by ICP–AES.

LA–ICP–MS zircon U–Pb dating

Zircons were extracted from whole-rock samples at the Hebei Institute of Regional Geology and Mineral Resources Survey, China. Zircons were mounted on an epoxy disk, carefully polished until the cores were exposed, and photographed by transmitted light, reflected light, and cathodoluminescence (CL). LA–ICP–MS U–Pb zircon geochronological analysis was performed at the Geological Laboratory Center, China University of Geosciences (Beijing). LA–ICP–MS was performed with a laser ablation sampling system (UP193SS, New Wave Research Inc., USA) and an Agilent 7500a quadrupole mass analyzer plasma mass spectrometer (Agilent Technologies, USA). Helium was used as carrier gas with a 36 μm spot size and a laser repetition rate of 10 Hz. Data acquisition time was 45 s. Zircon 91500 was used as standard to determine zircon U–Pb isotopic ratio and calibrate age. NIST612 and Si were used as external and internal standards in trace element analysis; NIST612 and NIST614 were used as monitor-blind samples. In the current study, $^{207}\text{Pb}/^{206}\text{Pb}$ ages (Paleoproterozoic) were utilized and calibrated using ^{204}Pb . The error of a single data point was 1σ , and the average weighted error was 2σ .

Rb–Sr and Sm–Nd isotopic analyses

Sr–Nd isotopic compositions were determined by ID-TIMS with a multi-collector Finnigan MAT-261 mass spectrometer at the Isotope Laboratory of the State Key Laboratory of Geological Processes and Mineral Resources, China University of Geosciences, Wuhan. Dissolution was performed using HNO_3 + HF mixture and an acid digestion bomb (190 °C, 48 h). Rb, Sr, and REEs in the dissolved sample were separated using an AG50 × 8 cation exchange resin. Nd was separated and purified using a special LN resin produced by Eichrom. We conducted the Sr/Nd isotope ratio measurements on the prepared sample by thermal ionization isotope mass spectrometry (TIMS, Triton TI). The accuracy of the instrument was monitored using NBS987 and La Jolla international standards. The mass fractionation of the Sr isotope was corrected with $^{88}\text{Sr}/^{86}\text{Sr} = 8.375209$. The $^{87}\text{Sr}/^{86}\text{Sr}$ ratio of the international standard NBS987 was 0.710240 ± 6 (2σ m, the same as parameter described in the following section). The mass fractionation of the Nd isotope was corrected with $^{146}\text{Nd}/^{144}\text{Nd} = 0.721900$. The $^{143}\text{Nd}/^{144}\text{Nd}$ ratio of the international standard La Jolla was 0.511844 ± 1 (2σ).

Results and discussions

Geochemical characteristics and tectonic backgrounds

Results of geochemical analyses are listed in Table 1.

The Dahalajunshan Formation volcanic rocks consist of basalt, basaltic andesite, andesite, basaltic trachyandesite, dacite, and rhyolite based on the whole-rock silica versus alkali classification (Fig. 4). The majority of the andesite contains pyroxene, as observed in the Axi gold mine where surrounding rocks (TST071-1) are pyroxene andesite. These rocks display porphyritic texture and massive structure. The porphyritic minerals are mainly represented by euhedral and hypidiomorphic tabular plagioclase, and a small amount of clinopyroxene which shows replacement by chlorite. The groundmass is fine andesitic lava.

The chondrite-normalized rare earth element patterns of the rocks are characterized by light rare earth element (LREE) enrichment and heavy rare earth element (HREE) depletion with a $(\text{La/Yb})_{\text{N}}$ varying from 1.74 to 23.03. $\delta\text{Eu} = \text{Eu}_{\text{N}}/(\text{Sm}_{\text{N}} \times \text{Gd}_{\text{N}})^{1/2}$ varies from 0.04 to 0.94 (Fig. 5; Table 1). Some samples exhibit a negative Eu anomaly. For mafic rocks, the older basalt (TST090-2, 359 Ma, Zhou et al. 2015) shows a moderate LREE enrichment and flat HREE pattern in the chondrite-normalized diagram with a slightly negative (rarely detected) Eu anomaly ($\delta\text{Eu} = 0.90$; Fig. 5a). However, the younger basalt (TS2101, 333 Ma) shows wing-shaped REE pattern with a marked negative Eu

Table 1 Major (%), rare earth and trace element (ppm) data of the Dahalajunshan Formation in West Tianshan, Xinjiang Uygur Autonomous Region

Sample	Petrography	SiO ₂	TiO ₂	Al ₂ O ₃	Fe ₂ O ₃	FeO	MnO	MgO	CaO	Na ₂ O	K ₂ O	P ₂ O ₅	LOI	SUM		
TST090-2	Altered basalt	50.08	1.22	16.03	3.26	6.67	0.45	8.44	6.17	2.83	1.42	0.19	3.12	99.89		
TST071-1	Basaltic andesite	54.71	1.29	16.95	4.26	4.09	0.17	3.62	4.55	3.46	2.23	0.31	4.08	99.71		
TST086-0	Dacite	74.15	0.34	13.83	2.29	0.24	0.05	0.27	0.30	4.44	2.84	0.08	0.87	99.71		
TST087-3	Dacite	77.80	0.21	12.35	1.46	0.19	0.04	0.49	0.39	3.34	2.70	0.04	0.85	99.85		
TST098-1	Andesitic porphyrite	69.90	0.50	15.64	3.14	0.11	0.03	0.42	0.94	2.70	4.20	0.16	1.97	99.71		
TST091-1	Dosemic rhyolite	72.10	0.35	15.88	1.69	0.25	0.01	0.36	0.15	4.23	3.15	0.02	1.55	99.74		
TST071-2	Andesitic clastic rock	77.37	0.52	11.84	2.67	0.28	0.04	0.41	0.39	0.10	3.44	0.12	2.60	99.78		
TST086-1	Dacite	70.46	0.61	14.89	2.94	0.23	0.11	0.81	0.64	3.95	3.70	0.14	1.31	99.79		
TST087-1	Andesite tuff	65.54	0.55	15.79	2.95	1.27	0.12	1.92	2.64	2.63	3.62	0.11	2.58	99.74		
TST087-2	Dacite	70.07	0.49	14.26	2.67	1.00	0.11	1.41	2.31	2.61	2.83	0.08	2.16	99.99		
TS17-2	Andesitic porphyrite	62.20	0.50	14.80	3.94			0.08	1.54	4.71	1.89	3.07	0.14	6.17	99.17	
TS31-2	Andesitic breccia	61.30	0.91	13.55	5.47			0.09	3.20	4.66	1.82	2.86	0.24	5.65	99.9	
TS35-3	Rhyolite	68.10	0.76	12.70	4.63			0.08	1.62	4.80	2.66	1.43	0.16	2.49	99.57	
TS35-4	Andesite tuff	61.00	1.0	13.60	5.61			0.10	2.99	4.41	2.01	2.71	0.24	5.54	99.25	
TS35-5	Andesite tuff	61.50	0.58	18.75	3.39			0.08	4.81	0.58	1.80	3.11	0.10	5.27	100.1	
TS35-6	Andesite tuff	61.50	0.56	18.05	3.2			0.09	4.79	0.48	2.09	3.17	0.08	5.20	99.34	
TS35-7	Basaltic trachyandesite	53.50	0.78	15.25	6.52			0.10	4.09	5.71	3.74	1.36	0.17	7.05	101.15	
TS21-1	Basalt	51.70	1.22	16.05	10.29			0.15	5.56	4.82	3.35	2.72	0.25	3.40	99.74	
TS23-1	Rhyolite	77.80	0.06	11.65	0.91			0.01	0.03	0.21	3.14	5.21	0.01	0.29	99.34	
TS23-3	Rhyolite	79.60	0.05	11.00	0.79			0.01	0.02	0.20	3.44	4.17	0.01	0.44	99.74	
TS23-4	Rhyolite	78.30	0.06	11.35	0.66			0.01	0.03	0.16	2.87	5.40	0.01	0.46	99.34	
TS23-5	Rhyolite	81.60	0.05	9.70	0.69			0.01	0.02	0.13	2.29	4.92	0.01	0.40	99.83	
TS23-7	Rhyolite		77.40	0.06	12.35	0.52			0.01	0.03	0.19	3.71	4.88	0.01	0.36	99.57
TS32-1	Massive lava		74.10	0.22	12.25	1.52			0.05	0.31	1.32	3.28	3.92	0.06	1.89	99.04
TS32-5	Massive lava		74.20	0.24	13.20	1.58			0.03	0.30	0.83	3.39	4.23	0.07	1.58	99.76
Sample	La	Ce	Pr	Nd	Sm	Eu	Gd	Tb	Dy	Ho	Er	Tm	Yb	Lu	Y	La/Yb
TST090-2	5.46	18.16	2.96	14.29	3.98	1.23	4.39	0.81	5.43	1.07	3.05	0.49	3.14	0.45	28.15	1.74
TST071-1	30.18	64.78	8.02	31.93	6.65	1.66	6.23	1.03	6.26	1.25	3.51	0.56	3.59	0.53	33.69	8.41
TST086-0	22.69	50.59	6.67	26.53	5.82	1.04	5.52	1.07	6.84	1.42	4.35	0.75	5.03	0.77	42.44	4.51
TST087-3	21.89	44.20	5.17	18.88	3.79	0.70	3.68	0.69	4.51	0.95	2.85	0.48	3.31	0.50	27.67	6.61
TST098-1	36.50	71.95	8.12	28.29	4.86	1.25	4.15	0.66	3.69	0.71	2.15	0.36	2.41	0.36	20.78	15.15
TST091-1	1.58	2.86	0.42	1.75	0.43	0.11	0.47	0.10	0.87	0.21	0.72	0.15	1.18	0.21	5.94	1.34
TST071-2	33.16	77.06	9.50	35.45	6.01	1.32	5.18	0.84	4.93	0.97	2.82	0.47	3.03	0.46	26.94	10.94
TST086-1	30.11	63.33	7.79	30.30	6.28	1.40	5.85	1.00	6.26	1.28	3.74	0.63	4.16	0.62	36.82	6.96
TST087-1	19.71	46.20	5.85	22.64	4.56	1.26	4.10	0.71	4.31	0.85	2.50	0.41	2.83	0.39	23.41	7.31
TST087-2	18.49	39.53	4.82	18.09	3.68	0.96	3.37	0.58	3.70	0.75	2.21	0.37	2.53	0.37	20.32	11.54
TS17-2	15.0	33.8	3.60	13.6	2.60	0.8	2.6	0.4	2.2	0.42	1.30	0.19	1.30	0.20	12.2	8.01
TS31-2	20.1	49.30	5.30	20.9	4.60	1.3	4.83	0.8	4.42	0.88	2.60	0.40	2.51	0.38	26.0	11.31
TS35-3	31.1	68.10	7.64	29.5	5.93	1.34	5.8	0.85	4.97	1.0	2.93	0.42	2.75	0.40	30.4	9.09
TS35-4	21.9	50.40	5.46	21.6	4.55	1.2	4.72	0.71	4.2	0.84	2.50	0.36	2.41	0.36	24.7	5.58
TS35-5	19.1	50.40	6.00	24.3	5.18	1.25	5.42	0.83	5.1	1.05	3.30	0.50	3.42	0.53	26.9	4.10
TS35-6	15.4	39.80	4.51	18.9	4.63	1.2	5.5	0.92	5.72	1.2	3.76	0.56	3.76	0.60	32.4	8.71
TS35-7	18.3	41.40	4.63	18.4	3.99	1.1	4.12	0.61	3.64	0.73	2.21	0.31	2.10	0.32	21.8	9.35
TS21-1	12.0	32.4	4.15	18.3	4.91	1.21	5.80	0.95	5.97	1.23	3.82	0.57	3.93	0.60	37.9	9.90
TS23-1	19.5	48.8	4.71	17.1	3.66	0.06	3.19	0.51	2.97	0.59	1.85	0.29	1.97	0.30	17.9	10.09
TS23-3	22.2	51.4	5.68	20.3	4.16	0.05	3.72	0.60	3.51	0.69	2.11	0.33	2.20	0.32	20.2	10.48
TS23-4	24.0	55.4	6.10	22.1	4.73	0.06	4.15	0.62	3.57	0.71	2.20	0.34	2.29	0.35	20.0	9.01

Table 1 continued

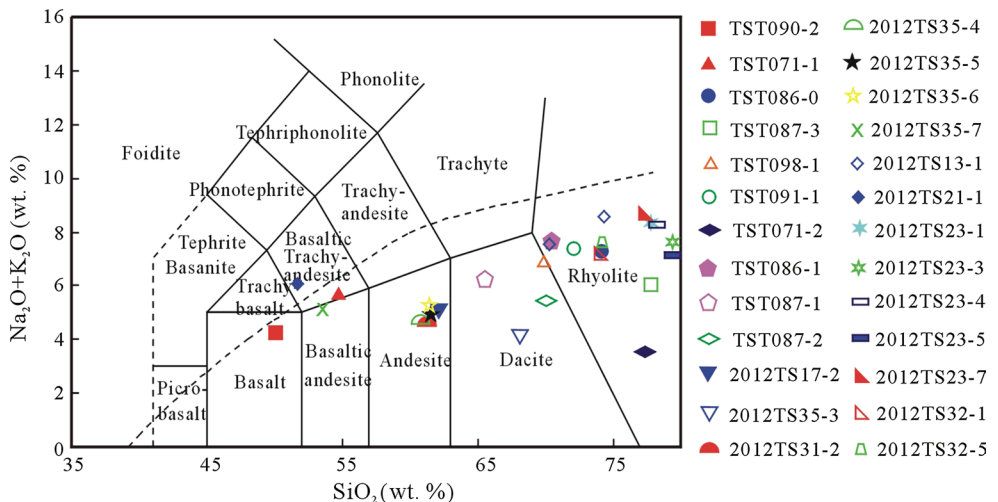
Sample	La	Ce	Pr	Nd	Sm	Eu	Gd	Tb	Dy	Ho	Er	Tm	Yb	Lu	Y	La/Yb
Sample	Cr	Cs	Rb	Ba	Th	U	Nb	Ta	Pb	Sr	P	Zr	Hf	Ti	Ga	$\delta\text{Eu}^{\text{a}}$
TS23-5	21.0	43.1	5.45	19.6	4.22	0.05	3.90	0.62	3.75	0.74	2.29	0.35	2.33	0.35	22.8	8.20
TS23-7	21.9	51.3	5.57	20.0	4.30	0.06	4.00	0.64	3.90	0.77	2.48	0.39	2.67	0.41	22.2	23.03
TS32-1	47.9	90.3	8.03	26.2	4.28	0.78	3.60	0.54	3.07	0.60	1.88	0.29	2.08	0.33	19.9	21.14
TS32-5	42.5	81.4	7.29	23.5	3.76	0.63	3.21	0.47	2.79	0.57	1.83	0.28	2.01	0.32	18.8	1.74
TST090-2	173.7	0.69	45.80	872.60	2.62	0.44	3.91	0.31	2.21	199.5	829.19	128.9	3.40	7311.9	14.96	0.90
TST071-1	28.00	4.07	57.60	577.00	10.49	2.86	25.18	1.69	11.91	422.0	1352.9	245.9	5.37	7731.5	22.14	0.79
TST086-0	3.30	1.11	49.30	754.60	13.42	2.54	14.51	1.08	9.00	83.40	349.13	311.9	7.53	2037.7	12.65	0.56
TST087-3	7.50	1.47	59.70	611.10	10.34	3.40	13.42	1.09	13.66	83.0	174.56	201.8	5.95	1258.6	11.23	0.57
TST098-1	7.20	4.25	169.70	536.30	19.31	5.51	16.95	1.49	9.05	190.2	698.27	308.8	7.09	2996.7	18.90	0.85
TST091-1	6.95	0.94	93.00	516.90	2.86	1.16	5.73	0.60	6.35	76.1	87.28	142.4	3.71	2097.7	13.30	0.75
TST071-2	3.30	7.75	94.70	1362.70	10.05	2.66	23.52	1.66	5.61	74.1	523.70	324.9	6.47	3116.5	13.88	0.72
TST086-1	5.90	1.55	101.50	888.60	14.17	2.83	14.11	1.01	11.08	177.1	610.98	323.7	7.35	3655.9	14.99	0.89
TST087-1	15.40	20.90	135.80	614.00	12.05	2.76	11.14	0.84	13.04	284.1	480.06	173.6	4.65	3296.3	16.02	0.83
TST087-2	10.40	15.08	109.60	566.60	10.85	2.61	9.18	0.75	14.62	288.3	349.13	166.7	4.31	2936.7	14.76	0.94
TS17-2	16.0	9.96	85.4	200.0	6.4	1.60	5.60	0.47	7.30	128.5	610.9	89.0	2.80	2996.7	17.70	0.84
TS31-2	10.0	22.5	118.5	470	8.20	2.80	11.7	0.93	17.1	114.5	1047	162.5	4.6	5454.0	16.6	0.70
TS35-3	33.0	2.7	70.0	270.0	12.4	3.50	16.2	1.16	19.1	241	698.2	191.5	5.5	4555.0	18.15	0.79
TS35-4	11.0	23.0	113.0	340	8.0	3.30	12.0	1.0	17.4	105.5	1047	160.5	4.5	5993.4	15.85	0.72
TS35-5	3.00	26.8	61.5	440	9.6	1.20	16.3	1.42	22.3	38.2	436.4	293	9.0	3476.1	23.9	0.73
TS35-6	3.00	32.3	62.7	460	8.70	1.30	16.7	1.36	25.8	35.7	349.1	296	8.8	3356.3	21.8	0.83
TS35-7	62.0	3.52	57.7	70	5.5	1.40	6.7	0.51	11.1	230	741.9	150.5	4.1	4674.8	19.1	0.56
TS21-1	16.0	8.06	266	750	4.5	1.3	10.6	0.72	21.8	374	1050	157.0	4.9	7311.9	20.6	0.05
TS23-1	1.0	2.69	190.5	50	21.5	3.4	28.1	2.13	35.6	31.3	30	115.0	4.9	359.6	17.10	0.04
TS23-3	1.0	1.88	173.0	40	21.1	3.9	26.9	2.17	40.0	24.4	20	113.5	5.1	299.6	15.10	0.04
TS23-4	2.0	1.78	197.5	100	22.8	3.2	25.5	2.19	27.5	32.3	40	114.0	5.3	359.6	16.25	0.04
TS23-5	1.0	2.06	198.5	50	19.0	3.1	21.1	1.80	24.7	16.8	30	106.0	4.7	299.6	14.55	0.04
TS23-7	1.0	1.54	196.0	70	23.1	4.0	30.0	2.21	21.7	33.6	30	140.5	6.2	359.6	15.60	0.61
TS32-1	1.0	6.34	140.0	700	22.4	3.8	29.1	2.57	14.8	102.5	290	82.3	2.9	1318.5	14.30	0.55
TS32-5	1.0	6.52	143.0	710	21.5	3.7	29.0	2.57	13.7	92.0	280	82.3	3.0	1438.4	14.20	0.90

^a δEu ($=\text{EuN}/(\text{SmN} \times \text{GdN})^{1/2}$)

anomaly ($\delta\text{Eu} = 0.05$; Fig. 5a). From the felsic rocks, two rhyolite samples (TS23-5 and TS23-7) exhibit marked negative Eu anomaly (Fig. 5e), which is in contrast to the other rhyolites around the sampling point TS23. The primitive mantle-normalized spider diagrams are characterized by large ion lithophile element (LILE) enrichment and distinct negative Nb, Ta, Eu, Sr, P, and Ti anomalies (Figs. 5b, d, f) with a varied increasing trend from mafic to felsic rocks.

The models proposed for the genesis of the Dahala-junshan volcanic rocks include intraplate rift, rift trough, active continental margin, and/or arc basin system, among others. Based on lithologic characteristics, the Dahala-junshan volcanic rocks constitute a mixture of basalt, andesite, and rhyolite. These are primarily intermediate rocks with secondary intermediate-felsic rocks, which locally include a few mafic and felsic rocks. However, bimodal volcanic

Fig. 4 TAS and trace element rock classification diagram



rocks are rarely observed. These features do not match an extensional setting model. According to the trace element tectonic discrimination (Fig. 6a–d), in addition to the two basalts, the majority of intermediate-felsic rock samples in Dahalajunshan Formation also show features of volcanic arc. These results are consistent with the continental–marine sedimentary environment as inferred from the field relations. Therefore, the Dahalajunshan Formation is inferred to have formed in a continental margin arc setting (Shao et al. 2006; Shu et al. 2007; Xia et al. 2007; Dong et al. 2010; Han et al. 2010; Li et al. 2010b; Liu et al. 2013).

LA-ICP-MS zircon U-Pb geochronology

The sampling locations for geochronology are shown in Fig. 1. The dated samples include TS35-2 purple andesitic tuff, TS31-2 groundmass of andesitic volcanic breccia, TS32-2 gray-purple amaranthine massive lava, TS23-6 rhyolite, TS21-2 andesitic porphyry, TS26-1 weak-silicified volcanic rock (not chosen for geochemical analysis), TS13-2 monzogranite (not included in Table 1), and TS17 andesitic porphyrite. In combination with the results of previous studies, the dated samples cover the entire Dahalajunshan Formation in West Tianshan. Compared with previous results, the data presented in this study are based on precise analytical techniques and provide more comprehensive information. The results from zircon geochronology are listed in Table 2 and shown in Fig. 7. In addition, many published high-precision age data on Dahalajunshan Formation volcanic rocks are given in Table 3.

Previous studies reported whole-rock Rb-Sr ages 351 ± 2 Ma (Li et al. 2008) in volcanic rock samples from the top boundary of Dahalajunshan Formation at Tekes area ($81^{\circ}52'E$) and near the unconformity surface of the upper Akeshake Formation. The zircon U-Pb ages 354 and

340 Ma of granite and granite porphyry veins, respectively, that invade Dahalajunshan Formation along the southern slope in Southeastern Zhaosu ($81^{\circ}16'E$) (Li et al. 2010a), are considered as the upper age limit of Dahalajunshan Formation in the western segment. Niu et al. (2010) and Yang et al. (2012) reported SHRIMP U-Pb zircon age 310 Ma of the quartz diorite porphyry invading Dahalajunshan Formation in the Awulale Mountain (near $87^{\circ}30'E$), which is likely the upper limit of the age of the Dahalajunshan Formation in the eastern portion of the West Tianshan deposition. However, the lower age limit of Dahalajunshan Formation is debated. Some workers reported Late Devonian U-Pb zircon ages from the western segment of West Tianshan (Zhu et al. 2005a, 2006b; Zhai et al. 2006; Jin 2010; Li et al. 2010a). The present study also obtained U-Pb zircon ages 367 Ma (TS31-2) to 376 Ma (TS 32-2) from the Dahalajunshan Formation rocks surrounding the Axi gold deposit occurring within continental volcanic setting. From west to east of the Yili Block, the ages of Dahalajunshan Formation volcanic rocks show a gradual transition from Late Devonian to the Early Carboniferous. The age of the monzonitic granite (TS13-2) that invades the Dahalajunshan Formation in east Xinyuan County is 322.2 ± 2.9 Ma, which is between Middle and Late Carboniferous. This finding indicates that the volcanic eruption of Dahalajunshan Formation in the middle–east segment of West Tianshan culminated before Late Carboniferous.

This is the first study that reports U-Pb zircon age 407 Ma from andesitic conglomerate (Table 2; Fig. 7) from the extreme northwestern domain (sample TS35-2 from the upper reaches of Lucaogou River, west of Sayram Lake, Yining City). This Early Devonian age is different from the other ages (such as those obtained from northeast of Yining area) of Dahalajunshan Formation. Although a time gap is observed between this age and the continuous active duration of the Dahalajunshan Formation, this result is

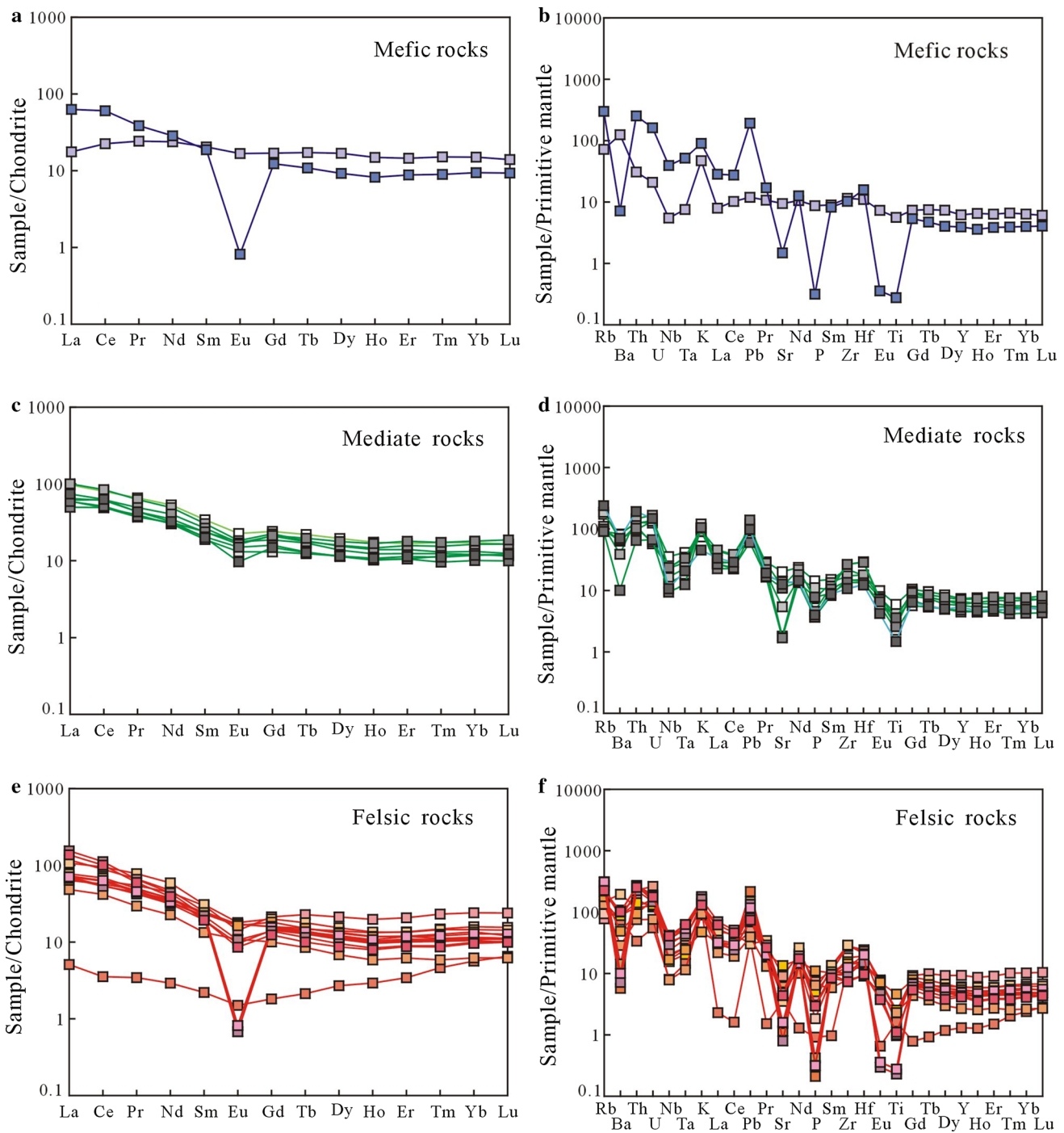


Fig. 5 Primitive mantle-normalized trace element spider diagrams and chondrite-normalized REE patterns

consistent with the ages 417–356 Ma reported by An et al. (2013) from Dahalajunshan Formation volcanic rocks in the west of Yining region. Thus, the andesitic conglomerate from locality TS35-2 may belong to Dahalajunshan Formation. Considering the single age of 407 Ma and the time gap, we infer that the volcanic activity began at

407 Ma and continued from the Late Devonian to the Middle Carboniferous.

Thus, according to the isotopic age data presented in Fig. 7 and Tables 2 and 3, the age of formation of Dahalajunshan Formation shows a roughly continuous decreasing trend from the west (376–367 Ma) to the east (310 Ma).

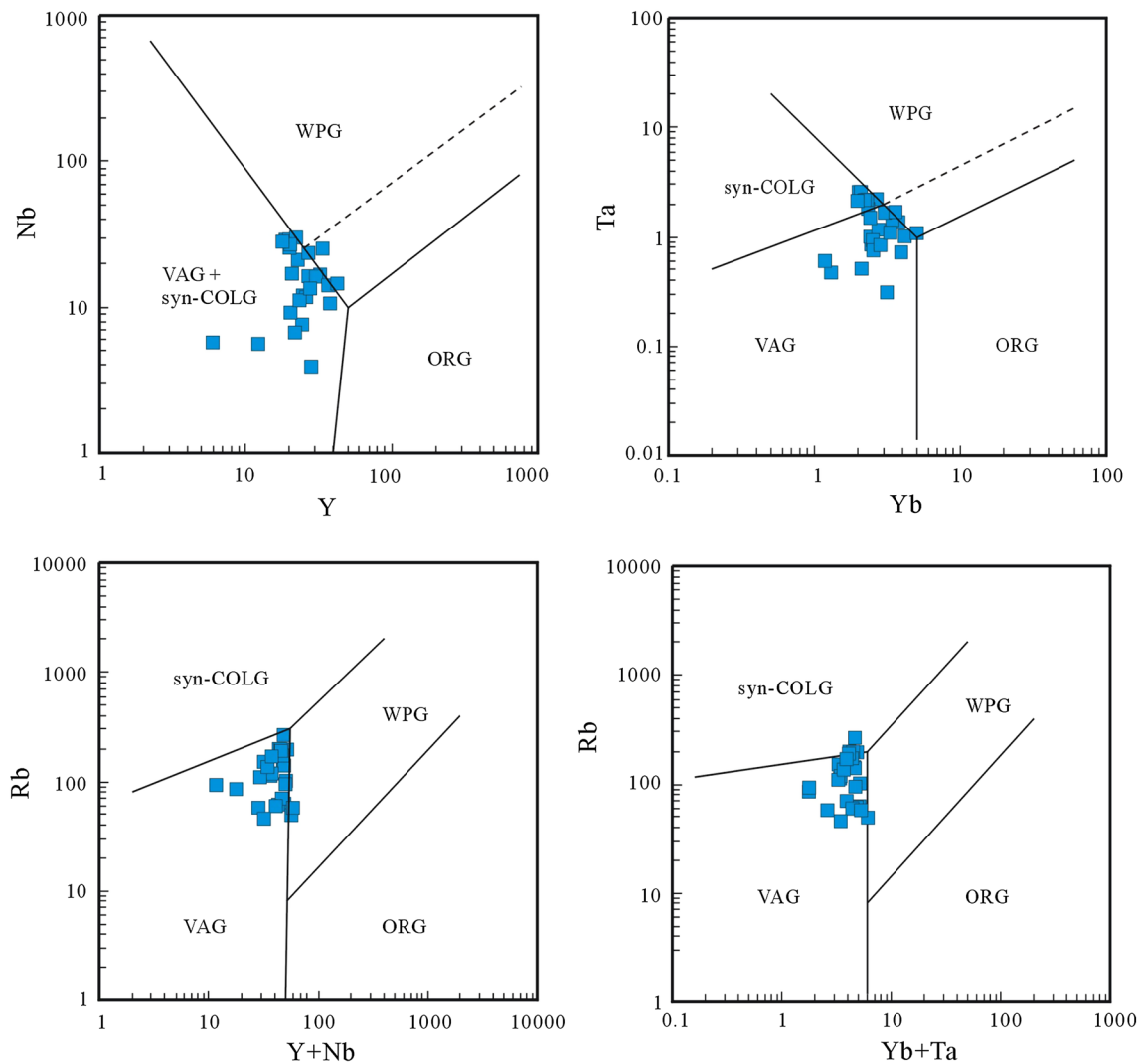


Fig. 6 Diagrams to discriminate the tectonic environment of the Dahalajunshan Formation volcanic rocks

Moreover, the rocks located in the northern part of Yili Block (376–367 Ma) are slightly earlier than those rocks in southern margin (364–333 Ma).

The younging from west to east can be attributed to subduction and collision processes of the South Tianshan Ocean, which gradually occurred from west to east in the Central Asian Orogenic Belt. The Dahalajunshan volcanic rocks in the northwest part of Yili Block may imply that the northward subduction must have been initiated in the Early Devonian and that the rocks in south part and east of Yili Block must have been produced by northward subduction of the South Tianshan Ocean during Late Devonian to Middle Carboniferous. Based on the age data, our conclusion is that the Dahalajunshan Formation volcanic rocks need not be subdivided into several formations.

Rb–Sr and Sm–Nd isotopic characteristics

As shown in Fig. 8, we collected 23 samples from five profiles for Rb–Sr and Sm–Nd isotopic analyses but although only 16 samples yielded good results as given in Table 4. We also synthesized the data from 15 samples from three profiles in the Awulake area (Li 2012), 10 samples from Laerdundaban (Qiaoerma) (Ai 2009), and 13 samples from two profiles in Southern Xinyuan County and the Laerdundaban region (Zhu et al. 2006b). Ai (2009) and Li et al. (2006) did not carry out Rb–Sr and Sm–Nd isotopic analysis. Zhu et al. (2006b) provided supplementary samples for regional analysis.

The Dahalajunshan Formation volcanic rocks are characterized by a typical continental arc geochemistry. A continental arc environment is favorable for interaction between oceanic crust and mantle materials (Chen et al.

Table 2 LA–ICP–MS zircon U–Pb analyses for the Dahalajunshan Formation in West Tianshan, Xinjiang Uygur Autonomous Region

Samples	Element contents			Isotopic ratios						Isotopic ages (Ma)					
	Th (ppm)	U (ppm)	Th/U	$^{207}\text{Pb}/^{206}\text{Pb}$		$^{207}\text{Pb}/^{235}\text{U}$		$^{206}\text{Pb}/^{238}\text{U}$		$^{207}\text{Pb}/^{206}\text{Pb}$		$^{207}\text{Pb}/^{235}\text{U}$		$^{206}\text{Pb}/^{238}\text{U}$	
				Val.	1 σ	Val.	1 σ	Val.	1 σ	Val.	1 σ	Val.	1 σ	Val.	1 σ
<i>TS35-2, conglomeratic andesite, Lucaogou, west to Yining</i>															
TS35-2-2	432	816	0.53	0.0532	0.0033	0.4737	0.0281	0.0648	0.0014	345	143	394	19.4	405	8.33
TS35-2-3	511	1207	0.42	0.0636	0.0037	0.5792	0.0328	0.0652	0.0010	731	122	464	21.1	407	5.98
TS35-2-4	273	473	0.58	0.0586	0.0054	0.5518	0.0594	0.0658	0.0022	550	199	446	38.9	411	13.24
TS35-2-5	208	573	0.36	0.0556	0.0043	0.5090	0.0375	0.0664	0.0015	435	172	418	25.3	414	8.94
TS35-2-6	298	805	0.37	0.0541	0.0035	0.4863	0.0309	0.0654	0.0014	376	144	402	21.1	409	8.45
TS35-2-7	887	1485	0.60	0.0516	0.0023	0.4607	0.0205	0.0640	0.0010	333	102	385	14.3	400	6.11
TS35-2-8	425	1252	0.34	0.0533	0.0023	0.4975	0.0204	0.0669	0.0011	343	96.3	410	13.9	417	6.55
TS35-2-9	637	923	0.69	0.0560	0.0030	0.5171	0.0276	0.0657	0.0010	454	119	423	18.5	410	6.16
TS35-2-11	272	577	0.47	0.0538	0.0034	0.4927	0.0290	0.0651	0.0012	365	143	407	19.8	407	7.38
TS35-2-12	255	541	0.47	0.0547	0.0039	0.5006	0.0346	0.0655	0.0012	398	159	412	23.4	409	7.26
TS35-2-13	274	717	0.38	0.0555	0.0039	0.4985	0.0326	0.0655	0.0012	432	128	411	22.1	409	7.52
TS35-2-15	463	641	0.72	0.0553	0.0057	0.4885	0.0507	0.0647	0.0021	433	233	404	34.6	404	12.66
TS35-2-16	576	1403	0.41	0.0544	0.0029	0.4820	0.0233	0.0643	0.0011	387	119	399	16.0	402	6.44
TS35-2-17	1157	2046	0.57	0.0548	0.0025	0.4975	0.0222	0.0653	0.0010	406	100.0	410	15.1	408	6.33
TS35-2-18	258	556	0.47	0.0550	0.0036	0.4882	0.0304	0.0643	0.0013	413	148	404	20.8	402	7.92
TS35-2-21	308	563	0.55	0.0579	0.0039	0.5207	0.0339	0.0659	0.0014	524	182	426	22.6	411	8.22
TS35-2-22	782	1674	0.47	0.0563	0.0024	0.5261	0.0241	0.0671	0.0012	465	101	429	16.0	419	7.04
TS35-2-23	885	1941	0.46	0.0546	0.0026	0.4851	0.0213	0.0646	0.0010	394	106	402	14.6	404	6.24
TS35-2-24	672	1068	0.63	0.0538	0.0025	0.4793	0.0213	0.0641	0.0010	365	104	398	14.6	400	6.31
TS35-2-25	172	384	0.45	0.0562	0.0048	0.4889	0.0374	0.0650	0.0014	461	191	404	25.5	406	8.74
<i>TS31-2, volcanic breccia, Yining NNE</i>															
TS31-2-2	1155	976	1.18	0.0544	0.0039	0.4600	0.0299	0.0610	0.0012	387	163	384	20.8	382	7.47
TS31-2-3	298	344	0.87	0.0545	0.0060	0.4322	0.0405	0.0581	0.0016	391	248	365	28.7	364	9.45
TS31-2-4	1374	1231	1.12	0.0545	0.0031	0.4339	0.0246	0.0573	0.0013	391	132	366	17.4	359	8.14
TS31-2-5	546	634	0.86	0.0595	0.0047	0.4659	0.0344	0.0569	0.0016	587	142	388	23.9	357	9.67
TS31-2-6	242	459	0.53	0.0574	0.0049	0.4720	0.0375	0.0599	0.0016	506	189	393	25.9	375	9.83
TS31-2-7	554	848	0.65	0.0575	0.0040	0.4533	0.0310	0.0571	0.0013	522	154	380	21.7	358	7.83
TS31-2-8	566	578	0.98	0.0539	0.0049	0.4423	0.0376	0.0599	0.0014	369	206	372	26.4	375	8.67
TS31-2-9	459	562	0.82	0.0507	0.0041	0.4064	0.0324	0.0571	0.0014	228	187	346	23.4	358	8.42
TS31-2-10	762	1212	0.63	0.0461	0.0030	0.3693	0.0235	0.0578	0.0013	400	-249	319	17.4	362	7.89
TS31-2-11	1313	971	1.35	0.0494	0.0039	0.4125	0.0301	0.0599	0.0014	169	174	351	21.6	375	8.44
TS31-2-13	510	827	0.62	0.0526	0.0038	0.4294	0.0275	0.0581	0.0013	309	163	363	19.5	364	8.17
TS31-2-18	503	510	0.99	0.0638	0.0055	0.5214	0.0399	0.0591	0.0014	744	185	426	26.6	370	8.36
TS31-2-19	537	652	0.82	0.0570	0.0052	0.4706	0.0402	0.0597	0.0014	500	200	392	27.8	374	8.33
TS31-2-20	740	854	0.87	0.0573	0.0036	0.4757	0.0285	0.0595	0.0013	502	134	395	19.6	372	7.66
<i>TS32-2, andesitic lava, Yining NNE</i>															
TS32-2-1	1348	1345	1.00	0.0616	0.0033	0.5244	0.0283	0.0603	0.0015	661	116	428	18.9	377	9.39
TS32-2-2	1391	1383	1.01	0.0535	0.0031	0.4522	0.0245	0.0611	0.0010	350	130	379	17.1	382	6.14
TS32-2-3	1037	897	1.16	0.0557	0.0037	0.4630	0.0279	0.0607	0.0012	443	150	386	19.4	380	7.21
TS32-2-4	1307	1671	0.78	0.0534	0.0030	0.4513	0.0242	0.0605	0.0010	346	132	378	16.9	378	5.97
TS32-2-5	1251	1947	0.64	0.0535	0.0027	0.4533	0.0233	0.0601	0.0011	350	115	380	16.2	376	6.72
TS32-2-6	981	1234	0.79	0.0551	0.0033	0.4483	0.0259	0.0585	0.0011	417	135	376	18.2	366	6.53
TS32-2-7	1509	1787	0.84	0.0573	0.0028	0.4761	0.0223	0.0595	0.0010	506	106	395	15.4	373	6.28
TS32-2-8	561	826	0.68	0.0509	0.0032	0.4432	0.0278	0.0612	0.0012	239	153	372	19.6	383	7.28
TS32-2-9	1097	1309	0.84	0.0549	0.0030	0.4630	0.0247	0.0603	0.0009	409	122	386	17.2	377	5.57

Table 2 continued

Samples	Element contents			Isotopic ratios						Isotopic ages (Ma)					
	Th (ppm)	U (ppm)	Th/U	$^{207}\text{Pb}/^{206}\text{Pb}$		$^{207}\text{Pb}/^{235}\text{U}$		$^{206}\text{Pb}/^{238}\text{U}$		$^{207}\text{Pb}/^{206}\text{Pb}$		$^{207}\text{Pb}/^{235}\text{U}$		$^{206}\text{Pb}/^{238}\text{U}$	
				Val.	1 σ	Val.	1 σ	Val.	1 σ	Val.	1 σ	Val.	1 σ	Val.	1 σ
TS32-2-10	1100	1691	0.65	0.0521	0.0028	0.4391	0.0223	0.0607	0.0011	300	124	370	15.8	380	6.64
TS32-2-11	877	871	1.01	0.0562	0.0038	0.4791	0.0306	0.0614	0.0012	461	150	397	21.0	384	7.25
TS32-2-12	1199	1279	0.94	0.0526	0.0031	0.4245	0.0244	0.0582	0.0009	309	135	359	17.4	365	5.39
TS32-2-14	1008	1120	0.90	0.0532	0.0033	0.4411	0.0251	0.0604	0.0012	345	144	371	17.7	378	7.14
TS32-2-15	1159	1841	0.63	0.0569	0.0028	0.4809	0.0237	0.0607	0.0010	487	109	399	16.2	380	6.01
TS32-2-17	468	629	0.74	0.0615	0.0047	0.5311	0.0362	0.0620	0.0015	655	165	433	24.0	388	9.03
TS32-2-18	704	701	1.00	0.0570	0.0040	0.4576	0.0291	0.0587	0.0011	494	154	383	20.3	368	6.79
TS32-2-19	416	487	0.85	0.0559	0.0046	0.4641	0.0352	0.0606	0.0014	456	190	387	24.4	379	8.65
TS32-2-20	1370	2082	0.66	0.0513	0.0024	0.4230	0.0205	0.0588	0.0010	254	114	358	14.6	368	6.34
<i>TS23-6, rhyolite, Tekes-Gongliu</i>															
TS23-6-5	1352	2193	0.62	0.05417	0.00135	0.43004	0.01146	0.05757	0.00099	378	31	363	8.0	361	6.00
TS23-6-8	2374	3410	0.70	0.05391	0.00134	0.4417	0.01172	0.0594	0.00103	367	31	371	8.0	372	6.00
TS23-6-9	1407	2369	0.59	0.05394	0.00138	0.44232	0.01202	0.05946	0.00103	369	32	372	8.0	372	6.00
TS23-6-10	441	817	0.54	0.05367	0.00155	0.44472	0.01335	0.06009	0.00107	357	37	374	9.0	376	7.00
TS23-6-12	1457	2352	0.62	0.05381	0.00138	0.43041	0.01176	0.058	0.00101	363	32	363	8.0	363	6.00
TS23-6-13	552	1403	0.39	0.05393	0.00148	0.42762	0.01234	0.0575	0.00102	368	35	361	9.0	360	6.00
TS23-6-15	1600	2543	0.63	0.05385	0.00141	0.43376	0.01207	0.0584	0.00102	365	33	366	9.0	366	6.00
TS23-6-16	1852	2655	0.70	0.05375	0.00146	0.42356	0.01213	0.05714	0.00101	361	34	359	9.0	358	6.00
TS23-6-18	60	120	0.50	0.05407	0.00334	0.4276	0.02613	0.05734	0.00129	374	97	361	19.0	359	8.00
TS23-6-19	1225	1889	0.65	0.0569	0.00157	0.45548	0.01324	0.05805	0.00104	488	34	381	9.0	364	6.00
TS23-6-20	744	1583	0.47	0.05395	0.00151	0.41707	0.01229	0.05606	0.001	369	36	354	9.0	352	6.00
TS23-6-22	867	1464	0.59	0.05364	0.00148	0.43081	0.01249	0.05824	0.00104	356	35	364	9.0	365	6.00
TS23-6-24	1240	2178	0.57	0.05374	0.00148	0.43149	0.01254	0.05822	0.00104	360	35	364	9.0	365	6.00
<i>TS21-2, andesite, Tekes-Gongliu</i>															
TS21-2-2	601	803	0.75	0.0654	0.0063	0.4674	0.0486	0.0542	0.0023	787	204	389	33.6	340	14.32
TS21-2-3	600	872	0.69	0.0561	0.0040	0.4288	0.0297	0.0550	0.0013	457	155	362	21.1	345	7.93
TS21-2-4	497	776	0.64	0.0499	0.0039	0.3944	0.0288	0.0571	0.0012	191	170	338	21.0	358	7.42
TS21-2-5	398	601	0.66	0.0561	0.0050	0.3843	0.0314	0.0493	0.0014	457	193	330	23.0	310	8.30
TS21-2-6	594	737	0.81	0.0551	0.0046	0.4059	0.0310	0.0547	0.0016	417	187	346	22.4	344	9.87
TS21-2-7	349	508	0.69	0.0518	0.0042	0.3726	0.0291	0.0524	0.0013	276	189	322	21.5	329	7.84
TS21-2-8	599	969	0.62	0.0576	0.0042	0.4394	0.0304	0.0556	0.0013	517	157	370	21.4	349	8.06
TS21-2-9	79.1	210	0.38	0.0558	0.0080	0.3899	0.0480	0.0541	0.0019	456	322	334	35.1	340	11.68
TS21-2-11	806	955	0.84	0.0533	0.0057	0.3850	0.0410	0.0524	0.0016	339	244	331	30.1	329	9.53
TS21-2-12	190	289	0.66	0.0639	0.0086	0.4481	0.0543	0.0544	0.0025	739	289	376	38.1	341	15.52
TS21-2-13	348	555	0.63	0.0456	0.0037	0.3259	0.0259	0.0498	0.0012	Error		286	19.8	313	7.26
TS21-2-14	225	323	0.70	0.0682	0.0083	0.4641	0.0465	0.0504	0.0016	876	249	387	32.2	317	10.06
TS21-2-15	169	261	0.65	0.0582	0.0064	0.3922	0.0320	0.0510	0.0015	600	243	336	23.4	320	9.33
TS21-2-17	374	526	0.71	0.0564	0.0058	0.3795	0.0327	0.0514	0.0014	478	223	327	24.1	323	8.85
TS21-2-18	69.7	156	0.45	0.0627	0.0095	0.3899	0.0422	0.0481	0.0020	698	324	334	30.8	303	12.05
TS21-2-19	130	305	0.43	0.0526	0.0052	0.3683	0.0278	0.0510	0.0014	322	223	318	20.6	321	8.65
TS21-2-20	354	629	0.56	0.0526	0.0038	0.4282	0.0280	0.0575	0.0012	322	169	362	19.9	360	7.23
<i>TS26-1, andesite, Axi gold deposit</i>															
TS26-1-1	195	345	0.56	0.0677	0.0071	0.5844	0.0583	0.0620	0.0026	861	219	467	37.4	388	15.65
TS26-1-6	149	253	0.59	0.0653	0.0067	0.5302	0.0445	0.0602	0.0019	783	216	432	29.5	377	11.32
TS26-1-7	161	292	0.55	0.0649	0.0067	0.5179	0.0456	0.0614	0.0019	769	187	424	30.5	384	11.59
TS26-1-8	231	400	0.58	0.0659	0.0063	0.5777	0.0572	0.0618	0.0018	806	200	463	36.8	387	10.76

Table 2 continued

Samples	Element contents			Isotopic ratios						Isotopic ages (Ma)					
	Th (ppm)	U (ppm)	Th/U	$^{207}\text{Pb}/^{206}\text{Pb}$		$^{207}\text{Pb}/^{235}\text{U}$		$^{206}\text{Pb}/^{238}\text{U}$		$^{207}\text{Pb}/^{206}\text{Pb}$		$^{207}\text{Pb}/^{235}\text{U}$		$^{206}\text{Pb}/^{238}\text{U}$	
				Val.	1 σ	Val.	1 σ	Val.	1 σ	Val.	1 σ	Val.	1 σ	Val.	1 σ
TS26-1-9	349	485	0.72	0.0535	0.0043	0.4425	0.0328	0.0588	0.0013	350	179	372	23.1	369	7.76
TS26-1-10	243	449	0.54	0.0660	0.0058	0.5257	0.0407	0.0592	0.0015	807	188	429	27.1	371	9.27
TS26-1-11	289	448	0.64	0.0667	0.0057	0.5600	0.0441	0.0604	0.0015	831	178	452	28.7	378	8.97
TS26-1-12	385	658	0.58	0.0547	0.0040	0.4669	0.0297	0.0605	0.0013	398	167	389	20.6	379	7.80
TS26-1-15	154	294	0.52	0.0560	0.0084	0.4761	0.0759	0.0616	0.0027	450	339	395	52.2	385	16.67
TS26-1-16	253	469	0.54	0.0624	0.0064	0.5661	0.0454	0.0621	0.0017	687	225	456	29.5	388	10.03
TS26-1-17	187	420	0.45	0.0515	0.0048	0.4475	0.0322	0.0606	0.0013	261	217	376	22.6	379	7.90
TS26-1-18	313	654	0.48	0.0532	0.0041	0.4713	0.0307	0.0622	0.0012	339	176	392	21.2	389	7.50
TS26-1-19	198	393	0.50	0.0534	0.0042	0.4532	0.0315	0.0610	0.0016	346	175	380	22.0	382	9.52
TS26-1-20	253	366	0.69	0.0509	0.0044	0.4204	0.0328	0.0608	0.0015	239	197	356	23.5	381	9.00
TS26-1-21	179	376	0.48	0.0584	0.0052	0.4879	0.0404	0.0608	0.0016	543	192	403	27.6	380	9.87
TS26-1-22	388	613	0.63	0.0604	0.0051	0.4718	0.0399	0.0576	0.0012	617	185	392	27.5	361	7.62
TS26-1-23	2060	1180	1.75	0.0542	0.0027	0.4429	0.0215	0.0592	0.0009	376	111	372	15.1	371	5.76
TS26-1-25	689	1404	0.49	0.0623	0.0029	0.5056	0.0235	0.0586	0.0010	683	100.0	415	15.9	367	6.17
TS26-1-26	170	285	0.60	0.0544	0.0060	0.4389	0.0451	0.0593	0.0016	387	252	369	31.9	372	9.64
TS26-1-27	178	339	0.53	0.0570	0.0053	0.4481	0.0349	0.0586	0.0016	500	206	376	24.5	367	9.47
TS26-1-28	193	280	0.69	0.0570	0.0056	0.4537	0.0351	0.0603	0.0017	500	218	380	24.5	378	10.14
TS26-1-29	531	575	0.92	0.0587	0.0041	0.4807	0.0305	0.0588	0.0013	567	152	399	20.9	369	7.67
TS26-1-30	141	274	0.51	0.0654	0.0064	0.5260	0.0464	0.0593	0.0015	787	204	429	30.9	372	9.09
<i>TS17-1, dacite, Xinyuan forest farm</i>															
TS17-1-1	732	1087	0.67	0.0700	0.0061	0.5645	0.0500	0.0575	0.0016	928	180	454	32.4	361	10.05
TS17-1-3	396	604	0.66	0.0557	0.0047	0.4220	0.0355	0.0568	0.0012	439	189	357	25.4	356	7.18
TS17-1-4	290	361	0.80	0.0757	0.0062	0.5872	0.0454	0.0575	0.0016	1088	163	469	29.1	361	9.99
TS17-1-5	314	423	0.74	0.0680	0.0098	0.5276	0.0802	0.0588	0.0021	878	270	430	53.3	368	12.82
TS17-1-6	483	696	0.69	0.0548	0.0041	0.4260	0.0293	0.0579	0.0012	467	166	360	20.9	363	7.27
TS17-1-8	317	485	0.65	0.0595	0.0059	0.4690	0.0488	0.0571	0.0017	587	218	391	33.7	358	10.57
TS17-1-10	276	339	0.81	0.0651	0.0065	0.4912	0.0472	0.0548	0.0015	789	211	406	32.1	344	9.32
TS17-1-11	444	486	0.91	0.0691	0.0078	0.5565	0.0729	0.0582	0.0015	902	235	449	47.5	365	9.40
TS17-1-14	253	325	0.78	0.0561	0.0061	0.4161	0.0367	0.0573	0.0016	454	243	353	26.3	359	9.92
TS17-1-15	769	860	0.89	0.0509	0.0036	0.3839	0.0241	0.0561	0.0011	235	163	330	17.6	352	6.83
TS17-1-16	390	524	0.74	0.0561	0.0040	0.4358	0.0295	0.0567	0.0012	454	159	367	20.9	355	7.22
TS17-1-18	837	622	1.34	0.0568	0.0042	0.4345	0.0330	0.0541	0.0010	483	165	366	23.4	339	6.42
TS17-1-19	306	526	0.58	0.0534	0.0046	0.4010	0.0318	0.0557	0.0014	346	166	342	23.0	349	8.40
TS17-1-20	397	717	0.55	0.0629	0.0045	0.5180	0.0355	0.0597	0.0013	706	153	424	23.7	374	7.69
TS17-1-21	279	366	0.76	0.0593	0.0054	0.4911	0.0409	0.0593	0.0015	576	200	406	27.8	372	8.98
TS17-1-22	526	958	0.55	0.0511	0.0032	0.4043	0.0244	0.0573	0.0013	243	144	345	17.7	359	8.03
TS17-1-23	851	938	0.91	0.0487	0.0030	0.4045	0.0234	0.0595	0.0011	132	202	345	16.9	373	6.77
TS17-1-24	552	686	0.80	0.0554	0.0037	0.4615	0.0290	0.0599	0.0012	428	118	385	20.1	375	7.22
TS17-1-25	801	1187	0.67	0.0543	0.0034	0.4483	0.0294	0.0581	0.0012	383	141	376	20.6	364	7.38
<i>TS13-2, monzogranite, Xinyuan forest farm</i>															
TS13-2-2	282	353	0.80	0.05373	0.00158	0.3803	0.01157	0.05133	0.00088	360	39	327	9.0	323	5.00
TS13-2-4	202	323	0.63	0.05338	0.00181	0.36606	0.01266	0.04972	0.00089	345	46	317	9.0	313	5.00
TS13-2-5	199	341	0.58	0.05369	0.00204	0.38262	0.01463	0.05167	0.00095	358	53	329	11.0	325	6.00
TS13-2-6	115	201	0.57	0.0532	0.00196	0.37988	0.0141	0.05178	0.00095	337	51	327	10.0	325	6.00
TS13-2-7	106	185	0.57	0.0532	0.00206	0.37966	0.01487	0.05174	0.00093	337	56	327	11.0	325	6.00
TS13-2-12	142	250	0.57	0.05323	0.00175	0.37921	0.01267	0.05165	0.00093	339	44	326	9.0	325	6.00

Table 2 continued

Samples	Element contents			Isotopic ratios						Isotopic ages (Ma)					
	Th (ppm)	U (ppm)	Th/U	$^{207}\text{Pb}/^{206}\text{Pb}$		$^{207}\text{Pb}/^{235}\text{U}$		$^{206}\text{Pb}/^{238}\text{U}$		$^{207}\text{Pb}/^{206}\text{Pb}$		$^{207}\text{Pb}/^{235}\text{U}$		$^{206}\text{Pb}/^{238}\text{U}$	
				Val.	1 σ	Val.	1 σ	Val.	1 σ	Val.	1 σ	Val.	1 σ	Val.	1 σ
TS13-2-13	193	259	0.75	0.05309	0.00155	0.37543	0.01139	0.05128	0.00089	333	38	324	8.0	322	5.00
TS13-2-15	173	279	0.62	0.05663	0.00363	0.39265	0.02403	0.05029	0.00095	477	146	336	18.0	316	6.00
TS13-2-16	139	204	0.68	0.05338	0.00184	0.37874	0.01328	0.05144	0.00092	345	47	326	10.0	323	6.00
TS13-2-17	249	311	0.80	0.05291	0.00184	0.36985	0.01307	0.05069	0.00092	325	48	320	10.0	319	6.00
TS13-2-18	142	195	0.73	0.05306	0.00199	0.38072	0.01444	0.05202	0.00095	331	53	328	11.0	327	6.00
TS13-2-20	379	469	0.81	0.05308	0.00138	0.38379	0.01055	0.05243	0.00089	332	33	330	8.0	329	5.00
TS13-2-21	138	223	0.62	0.05293	0.00175	0.37638	0.0127	0.05156	0.00092	326	45	324	9.0	324	6.00
TS13-2-22	133	222	0.60	0.05277	0.00192	0.36466	0.01342	0.0501	0.00092	319	51	316	10.0	315	6.00
TS13-2-23	184	256	0.72	0.05282	0.00202	0.37444	0.01445	0.0514	0.00094	321	55	323	11.0	323	6.00

2013a, b). During the formation process of subduction zones, oceanic and terrestrial materials enter the asthenospheric mantle through the subduction zones. Crustal materials are transported into the mantle wedge, where island arc magmas can form by the partial melting of the mantle wedge (Chen et al. 2013b, 2013c). Several processes of subduction and collision occurred in the Central Asian Orogenic Belt and resulted in the deep subduction of oceanic (Zhang et al. 2003) and continental (Zhu and Ogasawara 2002a, b). Continental crustal materials can return to the surface through volcanic activities (Zhu and Ogasawara 2002a, b, 2004). The Dahalajunshan Formation volcanic eruptions developed gradually from west to east, with the northern part of the Yili Block being slightly older at the southern edge.

Zhu et al. (2006b) showed that the intermediate-felsic volcanic rocks from the upper part of the Dahalajunshan Formation section in southern Xinyuan County exhibit relatively lower $\epsilon_{\text{Nd}}(t)$ (-0.22 to $+0.87$) and highly variable initial $^{87}\text{Sr}/^{86}\text{Sr}$ ratios (0.7045 – 0.7068). The basalt from the lower part of the section has lower initial $^{87}\text{Sr}/^{86}\text{Sr}$ ratio with small variation range (0.7044 – 0.7059). The $\epsilon_{\text{Nd}}(t)$ value of basalt is high, but the range of the variation is large ($+0.89$ to $+3.04$). Furthermore, a marine sedimentary interlayer exists between basalt and intermediate-felsic volcanic rocks. All of these observations indicate a relatively large difference between the formation times of the basalt from the lower part of the section and the intermediate-felsic volcanic rocks from the upper part. In addition, differences are observed between geochemical characteristics of intermediate-felsic volcanic rocks and basalt (Table 1; Fig. 5). These differences imply that the magmatic source of intermediate-felsic volcanic rocks and basalt is distinctly different. Furthermore, the intermediate-felsic volcanic rocks may be attributed to magmatism during volcanic eruptions after collision (Zhu et al. 2006b).

The majority of $\epsilon_{\text{Nd}}(t)$ values are positive, suggesting that the source region of the volcanic rocks is depleted mantle (Hart 1984; Dapaolo and Daley 2000). However, those sample value of $\epsilon_{\text{Nd}}(t) < 0$ may be attributed to contamination by crustal components through crust–mantle mixing. Four samples from of the rocks surrounding the Axi gold deposit exhibit minor negative values (top of Table 4), coupled with an $\epsilon_{\text{Nd}}(t)$ value of -0.28 of andesite from Nileke Jilintai and -1.2 from Dunde iron ore deposit. These results indicate the participation of minor crustal materials in the Dahalajunshan Formation volcanic rocks at the northern part and east of Yili Block. A general characteristic of Phanerozoic granitic rocks in the Central Asian Orogenic Belt is the positive $\epsilon_{\text{Nd}}(t)$ (Han et al. 1997, 1998; Heinhorst et al. 2000; Hong et al. 2003). The Dahalajunshan Formation volcanic rocks exposed in the northeastern Yining, Laerdundaban (Zhu et al. 2006a; Ai 2009), and Awulale (Li 2012) areas exhibit lower initial $^{87}\text{Sr}/^{86}\text{Sr}$ ratios (0.7015 – 0.7063) and positive $\epsilon_{\text{Nd}}(t)$ values ($+0.53$ to $+6.00$), which are most likely the product of both differentiation from the depleted mantle and crust–mantle mixing. As given in Table 4, the volcanic rocks located in the northern part of the Yili Block exhibit slightly lower positive $\epsilon_{\text{Nd}}(t)$ values and relatively high initial $^{87}\text{Sr}/^{86}\text{Sr}$ values, which indicate that crustal growth has been primarily completed through island arc amalgamation; mantle-derived magma related to subduction is superimposed on the continental crust through the inland arc. The volcanic rocks in mid-east and southern regions (Laerdundaban, Xinyuan area) yield slightly high positive $\epsilon_{\text{Nd}}(t)$ values and relatively lower initial $^{87}\text{Sr}/^{86}\text{Sr}$ ratios (Figs. 8, 9; Table 4), suggesting that the magma was sourced from a more depleted mantle.

Temporal and spatial variations in the Sr–Nd isotope compositions of volcanic rocks of the Dahalajunshan Formation in West Tianshan demonstrate that the earlier source of continental arc volcanic rocks in the northern part of

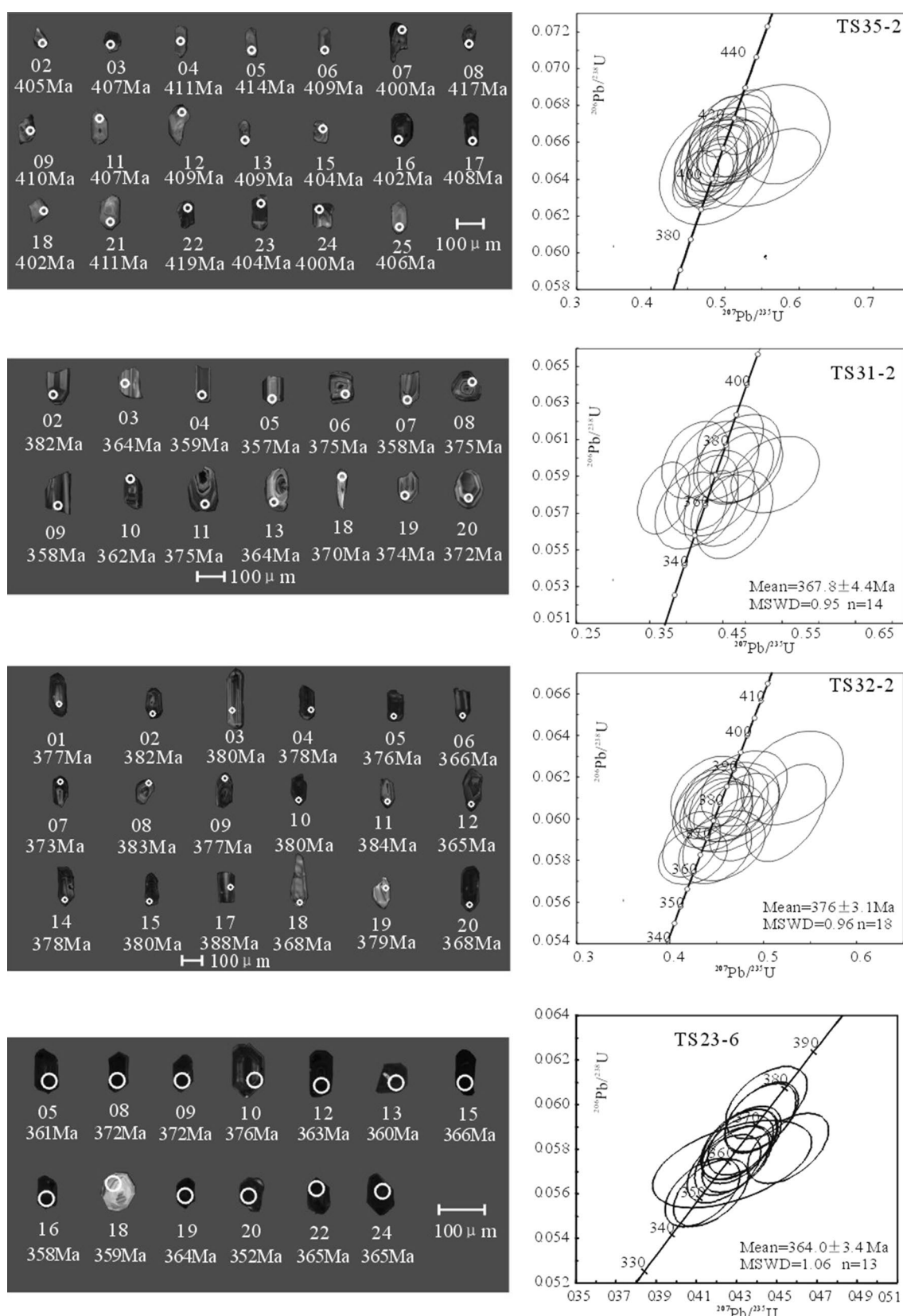


Fig. 7 Concordia plot of the LA-ICP-MS zircon U-Pb dating of the Dahalajunshan Formation volcanic rocks

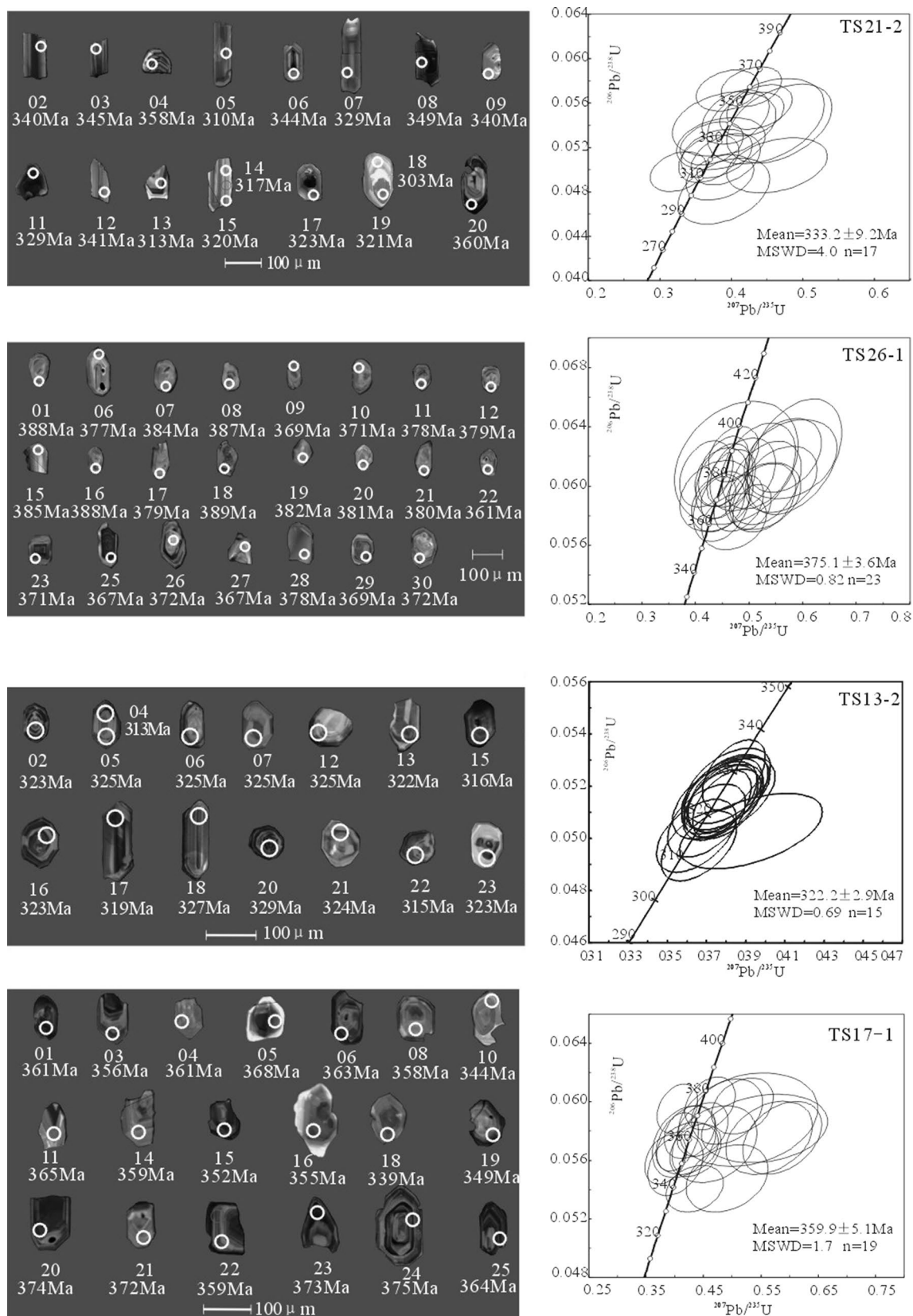


Table 3 Existing age data for the Dahalajunshan Formation in West Tianshan, Xinjiang Uygur Autonomous Region

Locations	Dating samples		Dating methods	Ages (Ma)	References
Axi gold deposit	Zircon	Quartz andesite	SHRIMP U–Pb	363.2 ± 5.7	Zhai et al. (2006)
Aladengtao Mts., southeast of Zhaosu County	Zircon	K-feldspar Granite	LA–ICP–MS	354	Li et al. (2010a, b)
South slope of Qiapuqiale mountain	Zircon	Granite porphyry	LA–ICP–MS	340	Li et al. (2010a, b)
Qiapu River, Yining area	Zircon	Light color dacite	LA–ICP–MS	333 ± 4	Li et al. (2011)
Northwestern Axi gold deposit	Zircon	Rhyolite	SHRIMP U–Pb	386–363	An and Zhu (2008)
Northwestern Axi gold deposit	Zircon	Rhyolite	SHRIMP U–Pb	417–356	An et al. (2013)
Tulasu basin	Zircon	Andesite	SHRIMP U–Pb	360.5 ± 3.4	Zhao et al. (2014)
Tulasu basin	Zircon	Andesite	LA–ICP–MS	347 ± 2	Tang et al. (2013)
Tulasu-Yelimodun	Zircon	Dacite	LA–ICP–MS	354.0 ± 1.3	Bai et al. (2011)
Wusun Mountain	Zircon	Ignimbrite	LA–ICP–MS	353.3 ± 3.5	Cheng et al. (2010)
Wusun Mountain	Zircon	Porphyritic Dacite	LA–ICP–MS	344 ± 6	Zhang et al. (2009)
Wusun Mountain	Zircon	Andesite	LA–ICP–MS	353.9 ± 6.5	Ru et al. (2012)
Wusun Mountain	Zircon	Andesitic tuff lava	LA–ICP–MS	356.3 ± 4.4	Ru et al. (2012)
Tekes forest farm	Pyroxene	Gabbroporphyrite	Ar–Ar	326	Liu et al. (1994)
Tekesdaban	Total rock	Rhyolite	Rd-Sr	351 ± 2	Liu (2007)
Kekesu River	Zircon	Andesitic basalt	LA–ICP–MS	358.9 ± 2.3	Li et al. (2012a, b)
Xinyuan northwest	Zircon	Basalt	SHRIMP U–Pb	354	Zhu et al. (2005a, b)
Kuerku-Lasitai	Total rock	Dacite	Rd-Sr	337	Li (2005)
Awulale mountain	Total rock	Dacite	Rd-Sr	351	Li et al. (2009a, b)
Awulale mountain	Zircon	Rhyolite	LA–ICP–MS	316.1 ± 2.2	Li et al. (2012b)
Beizhan iron deposit	Zircon	Dacite	LA–ICP–MS	329.1 ± 1.0	Sun et al. (2012)
Dunde iron deposit	Zircon	Dacite	LA–ICP–MS	316.0 ± 1.7	Duan et al. (2014)
Dunde iron deposit	Zircon	Andesite	LA–ICP–MS	328.7 ± 2.1	Jiang et al. (2014)
Laerdundaban	Zircon	Trachyandesite	SHRIMP U–Pb	313	Zhu et al. (2006a, b)
Yuximolegai	Zircon	Quartzdiorite	SHRIMP U–Pb	310	Niu et al. (2010)
Lucaogou, west to Yining	Zircon	Andesite	SHRIMP U–Pb	407	This paper
NNE Yining	Zircon	Volcanic breccia	SHRIMP U–Pb	367	This paper
NNE Yining	Zircon	Andesitic lava	SHRIMP U–Pb	376	This paper
Tekes-Gongliu	Zircon	Rhyolite	SHRIMP U–Pb	364	This paper
Tekes-Gongliu	Zircon	Andesite	SHRIMP U–Pb	333	This paper
Axi gold deposit	Zircon	Altered andesite	SHRIMP U–Pb	375	This paper
Xinyuan forest farm	Zircon	Monzogranite	SHRIMP U–Pb	322	This paper
Xinyuan forest farm	Zircon	Dacite	SHRIMP U–Pb	359	This paper

Yili Block has a relatively high $^{87}\text{Sr}/^{86}\text{Sr}$ value and a lower $\epsilon_{\text{Nd}}(t)$ value [which fall entirely within the Sr–Nd isotope variations of the volcanic island arc of the Lesser Antilles (Figs. 8, 9; Table 4) (Macdonald et al. 2000)] because of the nature of subducted material (i.e., terrigenous sediment and fluid from the subduction zone). Low initial Sr isotope ratios and high positive $\epsilon_{\text{Nd}}(t)$ values of the volcanic rocks in the mid-east region and at the southern margin of the Yili Block (especially east of Xinyuan County) exclude the existence of terrigenous materials (Fig. 8, 9; Table 4). Temporal and spatial variations in the characteristics of the magma source reflect the variations in the subduction intensity of the South Tianshan Ocean across regions of West Tianshan from Late Devonian to Early Carboniferous.

The western section witnessed northward subduction in Late Devonian–Early Carboniferous. Although the volcanic activities in the east occurred after the subduction peak, the extension-related bimodal volcanic rocks had not yet developed regionally before the end of Carboniferous. Thus, the south Tianshan belt had not yet reached the rift stage before Late Carboniferous (Jiang et al. 1995; Zhu et al. 2006b).

Tectonic significance of Dahalajunshan Formation

The Central Asian Orogenic Belt is the largest area of newborn continental crust in the Phanerozoic. This region of continental crust has an area of approximately

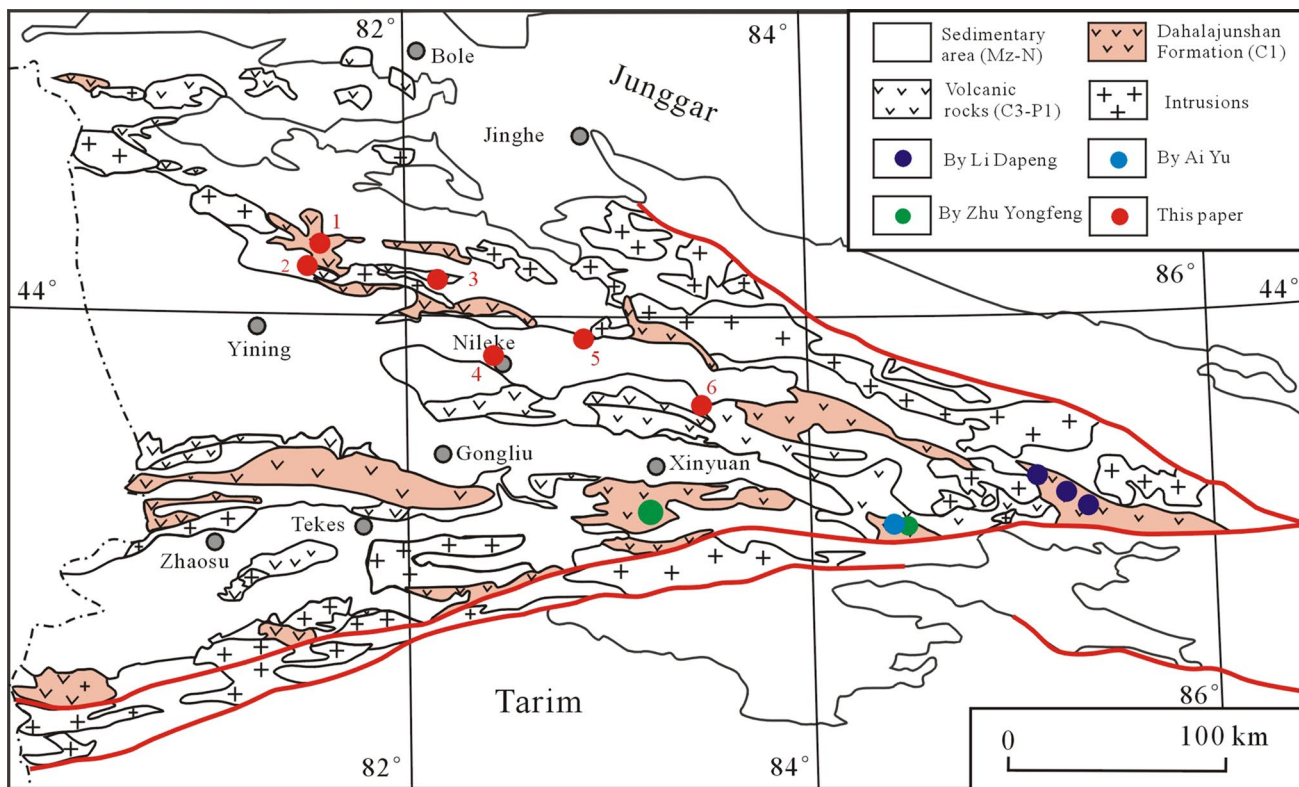


Fig. 8 Map showing the locations of the Sr–Nd samples in West Tianshan. 1 Axi gold deposit, 2 Panjin, Yining area, 3 Boerbosong River, Matuo Town, Yining area, 4 west of Nileke County, 5 Jilintai, east of Nileke County, 6 Barrier lake, north of Xinyuan County

5,000,000 km² formed through subduction, collision, and accretion along two major suture zones. The northern suture zone was finally formed in the late Carboniferous to early Permian (Xu et al. 2006), but it experienced an early subduction process during the Early Paleozoic. This early subduction process occurred during the Mid–Late Ordovician and ended in the Silurian, not only resulting in a unification of continental crust during the Early Paleozoic in North Tianshan by partial closure of multi-island oceanic basin of Kazakhstan–Junggar (including sutured Yili Block) but also creating a strong divergence in the south. This developed from a continental margin rift of the Late Ordovician or Early Silurian into a large-scale oceanic basin during the Mid–Late Paleozoic in South Tianshan (Li 1999; Tang 1995; Gao et al. 2006; Ma et al. 2007a; Chen et al. 2010; Xiao et al. 2013; Ma et al. 2014; Jiang et al. 2014; Klemd et al. 2015).

Many workers believed that the southern suture zone is the major suture zone of Tianshan (Allen et al. 1992; Gao et al. 2006, 2009; Windley et al. 2007; Han et al. 2011; Xiao et al. 2013; Ma et al. 2014; Jiang et al. 2014; Klemd et al. 2015) and that the glaucophane schist belt of At-Bashy–Kekesu–Nalati marks the most important suture zone in West Tianshan. This suture zone represents the final location of the closure of the south Tianshan Ocean

between Tarim and Junggar plates (including sutured Yili Block) (Allen et al. 1992; Gao and Klemd 2003; Gao et al. 2006, 2009; Xiao et al. 2004a, b, 2009; Windley et al. 2007; Zhang et al. 2007). Therefore, the subduction of the Southern Tianshan Ocean plays a major role in the formation of the Dahalajunshan volcanic rocks.

The South Tianshan Ocean underwent a long-term development from Late Ordovician (or Early Silurian) to Carboniferous and continuously expanded at least in Early Carboniferous. This ocean basin was closed in Late Carboniferous (Wang et al. 1994; He et al. 2001; Gao et al. 2006). In fact, the oceanic basin of South Tianshan experienced two major subduction events during closure. First, a southward subduction occurred during Silurian to middle Devonian. Second, a northward reversed subduction in the end of Late Devonian to Middle Carboniferous. The U–Pb age 407 Ma (this paper) for volcanic rocks belonging to the Dahalajunshan Formation in northwest of Yili Block may imply that the reversal from southward to northward subduction of the south Tianshan Ocean had initiated in the Early Devonian. Late Devonian to Middle Carboniferous island arc volcanic rocks of Dahalajunshan Formation may be products of the northward subduction of the South Tianshan Ocean (Yang et al. 2003; Li et al. 2006, 2008, 2010b; Sun et al. 2007; Wang et al. 2007; Yang et al. 2008;

Table 4 Sr and Nd isotope compositions of the Dahalajunshan Formation in West Tianshan, Xinjiang Uygur Autonomous Region

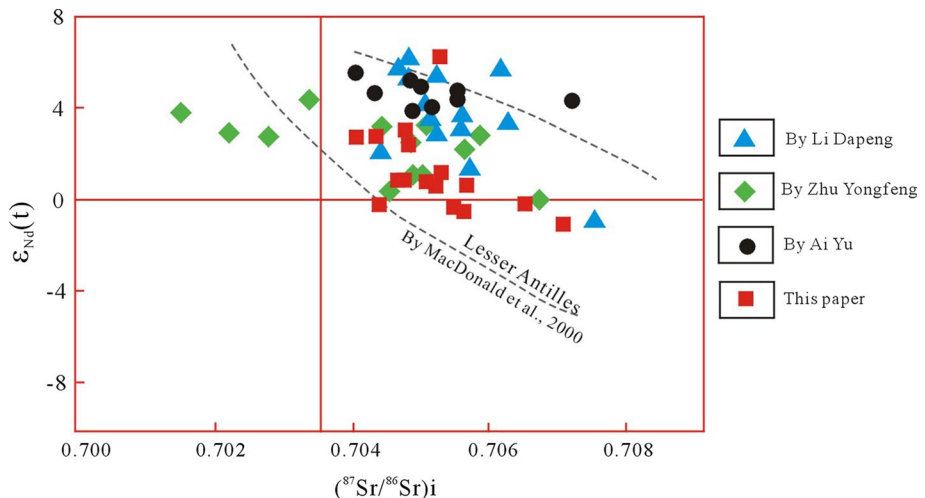
Sample	lithology	Age (Ma)	Rb (ppm)	Sr (ppm)	$^{87}\text{Rb}/^{86}\text{Sr}$	$^{87}\text{Sr}/^{86}\text{Sr}$	Sm (ppm)	Nd (ppm)	$^{147}\text{Sm}/^{146}\text{Sr}$	$^{143}\text{Nd}/^{144}\text{Nd}$	$^{143}\text{Nd}/^{144}\text{Nd}_{\text{di}}$	$\varepsilon_{\text{Nd}}(t)$	T _{DM}
<i>Axi gold deposit, Yining, spot 1 in Fig. 9, this paper</i>													
TST076-1	Andesitic porphyrite	375	50.2	167.4	0.869	0.711764	0.70712	6.85	31.54	0.131	0.512415	0.51209	-1.22 1.36
TST075-1	Andesite	375	138.4	177.9	2.255	0.717737	0.70570	7.16	38.16	0.113	0.512403	0.51212	-0.60 1.14
TST072-2	Andesite	375	97.1	94.8	2.969	0.721378	0.70552	4.77	22.95	0.126	0.512449	0.51214	-0.29 1.21
TST072-3	Implicit crystalline andesite	375	15.3	234	0.190	0.707581	0.70657	5.28	25.40	0.126	0.512451	0.51214	-0.24 1.21
<i>Panjin, Yining area, spot 2 in Fig. 9, this paper</i>													
TST071-1	Tuff lava	367	57.6	422	0.396	0.707785	0.70572	6.65	31.93	0.126	0.512495	0.51219	0.53 1.14
TST071-2	Tuff lava	367	94.7	74.1	3.705	0.723764	0.70441	6.01	35.45	0.102	0.512545	0.51230	2.60 0.83
TST071-4	Orthophyre	367	130.6	59.1	6.406	0.738708	0.70524	4.46	28.14	0.096	0.512428	0.51220	0.64 0.93
<i>Boerbosong river, Yining area, spot 3 in Fig. 9, this paper</i>													
TST083-1	Andesitic porphyrite	367	95.8	65.2	4.260	0.727596	0.70534	4.86	29.87	0.098	0.512455	0.51222	1.04 0.92
TST085-1	Andesitic porphyrite	367	102	88.5	3.341	0.722226	0.70477	7.13	37.97	0.114	0.512477	0.51220	0.76 1.03
<i>West of Nileke County, spot 4 in Fig. 9, this paper</i>													
TST086-0	Coarse grain andesite	354 ^a	49.3	83.4	1.714	0.713040	0.70440	5.82	26.53	0.133	0.512475	0.51217	-0.28 1.27
TST086-1	Andesitic lava	354 ^a	101.5	177.1	1.661	0.712459	0.70409	6.28	30.30	0.125	0.512606	0.51232	2.60 0.94
<i>Jilintai, east of Nileke County, spot 5 in Fig. 9, this paper</i>													
TST087-1	Conglomeratic andesite tuff	354 ^a	135.8	284.1	1.386	0.711660	0.70468	4.56	22.64	0.122	0.512516	0.51223	1.01 1.05
TST087-2	Dense andesite tuff	354 ^a	109.6	288.3	1.102	0.710684	0.70513	3.68	18.09	0.123	0.512497	0.51221	0.59 1.10
TST087-3	Fuchisia tuff	354 ^a	59.7	83	2.085	0.715376	0.70487	3.79	18.88	0.121	0.512581	0.51230	2.30 0.94
<i>Barrier Lake, north of Xinjiang County, spot 6 in Fig. 9, this paper</i>													
TST090-1	Pyroclastic rock	359	66.6	100.3	1.925	0.714651	0.70481	3.23	13.49	0.145	0.512667	0.51233	2.95 1.07
TST090-2	Basalt	359	45.8	199.5	0.6666	0.708710	0.70531	3.98	14.29	0.168	0.512889	0.51249	6.21 0.88
<i>Beizhan iron deposit, By Li (2012)</i>													
IP-002	Dacitic	320	33.6	494	0.197	0.706551	0.70566	6.13	28.00	0.132	0.512685	0.51241	3.5 0.9
IP-007	Dacitic	320	53.3	519	0.297	0.706458	0.70510	5.42	27.00	0.122	0.512678	0.51242	3.9 0.8
IP-008	Dacitic	320	27.3	580	0.136	0.706215	0.70560	5.66	25.90	0.132	0.512656	0.51238	3.0 0.9
IP-028	Dacitic	320	96.5	382	0.730	0.709631	0.70631	2.88	15.10	0.116	0.512631	0.51239	3.2 0.8
<i>Zhibo iron deposit, by Li (2012)</i>													
ZK009-10	Andesite	320	66.8	357	0.541	0.707124	0.70466	4.61	21.10	0.132	0.512780	0.51250	5.4 0.7
ZK009-11	Andesite	320	55.5	371	0.433	0.706628	0.70490	7.29	36.50	0.121	0.512746	0.51249	5.2 0.7
ZK009-15	Andesite	320	112.0	368	0.878	0.708854	0.70485	7.04	33.20	0.128	0.512800	0.51253	6.0 0.6
ZK009-19	Andesite	320	64.3	411	0.452	0.707247	0.70519	4.43	19.90	0.134	0.512777	0.51250	5.3 0.7
<i>Dunde iron deposit, by Li (2012)</i>													
DD-004	Basaltic tuff	320	77.2	270	0.828	0.709932	0.70616	6.54	27.60	0.143	0.512815	0.51252	5.6 0.7
DD-023	Basaltic tuff	320	47.4	298	0.461	0.707848	0.70575	6.64	35.00	0.115	0.512529	0.51229	1.2 1.0

Table 4 continued

Sample	lithology	Age (Ma)	Rb (ppm)	Sr (ppm)	$^{87}\text{Rb}/^{86}\text{Sr}$	$^{87}\text{Sr}/^{86}\text{Sr}$	$^{87}\text{Sr}/^{86}\text{Sr}_{\text{i}}$	Sr (ppm)	Nd (ppm)	$^{147}\text{Sm}/^{144}\text{Nd}$	$^{143}\text{Nd}/^{144}\text{Nd}$	$(^{143}\text{Nd}/^{144}\text{Nd})_{\text{di}}$	$\varepsilon_{\text{Nd}}(t)$	T _{DM}
<i>Qiaozema, By Ai (2009)</i>														
DD-035	Basaltic tuff	320	244.0	178	3.959	0.722482	0.70445	6.36	27.40	0.141	0.512623	0.51233	2.0	1.1
DD-058	Basaltic tuff	320	113.0	218	1.502	0.712001	0.70516	2.80	14.40	0.117	0.512646	0.51240	3.4	0.8
DD-066	Basaltic tuff	320	108.0	256	1.179	0.710630	0.70526	2.94	14.50	0.122	0.512613	0.51236	2.6	0.9
DD-030	Basaltic tuff	320	0.5	11.4	0.125	0.708151	0.70758	4.09	17.30	0.143	0.512464	0.51216	-1.2	1.5
DD-007	Basaltic tuff	320						5.22	22.2	0.142	0.51259	0.51229	1.3	1.2
<i>Xinyuan South, By Zhu et al. (2006b)</i>														
N01-27	Andesite	310	144.6	569	0.735	0.707592	0.70435	5.29	24.36	0.131	0.512739	0.51247	4.6	0.8
N01-29	Andesite	310	153.2	22.9	19.343	0.737308	0.65197	6.75	24.16	0.169	0.512839	0.51250	5.0	1.1
N01-38	Basalt	310	73.9	367	0.582	0.707454	0.70488	8.91	36.32	0.148	0.512804	0.51250	5.2	0.8
N01-45	Dacite	310	92.2	78.7	3.388	0.719029	0.70408	8.49	36.96	0.139	0.512803	0.51252	5.5	0.7
N01-46	Andesite	310	0.9	12.8	0.194	0.705773	0.70492	35.85	199.1	0.109	0.512653	0.51243	3.8	0.7
N01-47	Dacite	310	124.3	178	2.026	0.714141	0.70520	3.52	16.26	0.131	0.512710	0.51245	4.0	0.8
N01-48	Dacite	310	1.0	1438	0.002	0.705594	0.70558	0.54	5.80	0.056	0.512582	0.51247	4.5	0.6
N01-53	Rhyolite	310	0.6	39.9	0.045	0.705752	0.70556	2.55	9.67	0.159	0.512805	0.51248	4.7	1.0
N01-54	Basalt	310	0.8	489	0.005	0.707267	0.70725	4.47	20.84	0.130	0.512723	0.51246	4.3	0.8
N01-55	Basalt	310	127.2	526	0.699	0.708081	0.70500	5.30	22.34	0.143	0.512782	0.51249	4.9	0.8
TS76	Basalt	350	18.05	387.5	0.1344	0.705544	0.70487	3.05	11.68	0.1581	0.512670	0.51231	2.35	1.32
TS81	Altered andesite	350	43.95	622	0.2026	0.705981	0.70497	3.61	14.80	0.1480	0.512572	0.51223	0.89	1.34
TS88	Basalt	350	14.50	544.5	0.0765	0.706259	0.70588	4.51	18.05	0.1511	0.512674	0.51233	2.74	1.16
TS96	Trachyte andesite	350	46.74	235.1	0.5721	0.709616	0.70677	5.43	26.59	0.1235	0.512459	0.51218	-0.22	1.17
TS97	Trachyte andesite	350	75.34	592.4	0.3643	0.706880	0.70507	5.43	24.05	0.1367	0.512545	0.51223	0.87	1.20
TS107	Basalt	350	18.11	913.8	0.0571	0.705964	0.70568	5.31	19.28	0.1668	0.512677	0.51230	2.10	1.54
TS123	Basalt	350	92.36	813.3	0.3260	0.706076	0.70445	4.92	20.55	0.1449	0.512675	0.51234	3.04	1.05
TS131	Rhyolite	350	128.3	163.2	2.2937	0.715733	0.70450	3.00	13.78	0.1318	0.512506	0.51220	0.32	1.20
TS183	Trachyte	310	153.4	170.3	2.5860	0.715703	0.70282	4.69	21.34	0.1329	0.512646	0.51238	2.68	0.95
TS184	Trachyte	310	199.8	163.8	3.5170	0.719711	0.70219	5.63	23.20	0.1470	0.512682	0.51238	2.82	1.07
TS197	Trachyte	310	255.3	162.3	4.5360	0.724115	0.70152	4.24	18.58	0.1383	0.512719	0.51244	3.89	0.87
TS200	Trachyte	310	177.5	194.6	2.6220	0.716443	0.70338	5.38	24.27	0.1342	0.512731	0.51246	4.29	0.81
TS207	Trachyte andesite	310	255.1	1058	0.6938	0.708559	0.70512	79.20	17.06	0.1303	0.512660	0.50696	3.06	0.90

^a After Bai et al. 2011

Fig. 9 $\varepsilon_{\text{Nd}}(t)$ versus $(^{87}\text{Sr}/^{86}\text{Sr})_i$ diagram for the Dahalajunshan Formation volcanic rocks



Xiao et al. 2013; Ma et al. 2014; Jiang et al. 2014; Klemd et al. 2015; Scheltens et al. 2015). After oceanic crust was consumed in Mid–Late Carboniferous, collision occurred between the Tarim and Junggar plates (Shao et al. 2006; Gao et al. 2009). The formation ages of rocks changed in response to their locations. The age data reported in this paper and in previous studies indicate that some volcanic rocks of Dahalajunshan Formation in the north–northwest of Yili Block were formed in Early Devonian (Li et al. 2010b; Gao et al. 2009). Nevertheless, the majority of volcanic rocks of the Yining region were formed in the end of Late Devonian to Middle Carboniferous, especially in Early Carboniferous.

Although several workers insisted that the closure of South Tianshan Ocean occurred through southward subduction (Wang et al. 2009, 2010, 2014; Charvet et al. 2011; Tang et al. 2012, 2013; An et al. 2013), our study around the Yili Block and Kyrgyz Tianshan for the past couple of years attest to the northward subduction model presented by some workers (Gao et al. 1997, 2009; Huang et al. 2005; Qian et al. 2009; Han et al. 2011; long et al. 2013; Xiao et al. 2013, 2014a, b; Xu et al. 2013; Jiang et al. 2014, 2015; Xiao and Santosh 2014; Ma et al. 2014; Klemd et al. 2015). In summary, the Dahalajunshan Formation volcanic rocks represent the hall mark of Late Devonian–Middle Carboniferous tectonic events in West Tianshan. Temporal and spatial differences in formation age suggest that the South Tianshan Ocean gradually closed from west to east.

Conclusions

1. The volcanic rocks of Dahalajunshan Formation are products of the northward subduction of the South Tianshan Ocean in Late Paleozoic, which erupted from

Late Devonian to Middle Carboniferous from west to east. Their isotopic ages are broadly continuous.

2. The volcanic rocks of Dahalajunshan Formation are composed of basalt, basaltic andesite, andesite, trachy-andesite, and rhyolite. Early-stage volcanic rocks display continental facies and later-stage rocks gradually transformed into marine facies. The geochemical characteristics indicate that Dahalajunshan Formation is mainly composed of arc-related volcanic rocks which formed in a continental margin arc setting during the progressive closure of the south Tianshan oceanic basin during Late Paleozoic.
3. The Sr–Nd isotopic characteristics indicate that the volcanic rocks of Dahalajunshan Formation primarily originated from depleted magma with regional contributions of melted marine sediments.

Acknowledgments This study was financially supported by the Project of China Geological Survey (Grant No. 1212011120335 and 12120114006401). The major and trace elements were analyzed at the ALS Laboratory Group, Mineral Division - ALS Chemex. LA-ICPMS U–Pb zircon geochronological analysis was performed at the Geological Laboratory Center, China University of Geosciences (Beijing). Sm–Nd isotopic compositions were determined at the Isotope Laboratory of the China University of Geosciences (Wuhan). The authors thank Professor Jacques Charvet and other two anonymous reviewers for their insightful and detailed comments on the first version of the paper.

References

- Ai Y (2009) Petrological, geochemical and petrogenesis study of the Early Carboniferous volcanic rocks in Qiaoerma, West Tianshan. A Dissertation Submitted to China University of Geosciences for Master Degree, 1–50 (in Chinese with English abstract)
Allen MB, Windley BF, Zhang C (1992) Palaeozoic collisional tectonics and magmatism of the Chinese Tien Shan, central Asia. *Tectonophysics* 220:89–115

- An F, Zhu YF (2008) Study on trace elements geochemistry and SHRIMP chronology of volcanic rocks in Tulasu Basin, Northwest Tianshan. *Acta Petrol Sin* 24(12):2741–2748 (in Chinese with English abstract)
- An F, Zhu YF, Wei SN, Lai SC (2013) An Early Devonian to Early Carboniferous volcanic arc in North Tianshan, NW China: geochronological and geochemical evidence from volcanic rocks. *J Asian Earth Sci* 78:100–113
- Bai JK, Li ZP, Xu XY, Ru YJ, Li T (2011) The chronology of Tulasu-Yelmodun volcanic belt: constraints on the metallogenic epoch of the Jiamante gold deposit, Western Tianshan Mountains of Xinjiang. *Acta Geoscientica Sin* 32(3):322–330 (in Chinese with English abstract)
- Charvet J, Shu LS, Charvet SL, Wang B, Faure M, Cluzel D, Chen Y, Jong KD (2011) Palaeozoic tectonic evolution of the Tianshan belt, NW China. *Sci China (Earth Sci)* 54(2):166–184
- Che ZC, Liu L, Liu HF, Luo JH (1996) Review on the ancient Yili Rift, Xinjiang, China. *Acta Petrol Sin* 12(3):478–490 (in Chinese with English abstract)
- Chen G, Zhu ZX, Dong LH, Liu B, Ni XY, Zhao HL (2010) Determination and geological significance of ocean island volcanic rocks of the Devonian-early Carboniferous in Taxkorgan Region, Southern Tianshan of Xinjiang. *Xinjiang Geol* 28(3):236–241 (in Chinese with English abstract)
- Chen Y, Ye K, Guo S, Wu TF, Liu JB (2013a) Multistage metamorphism of garnet orthopyroxenites from the Maowu mafic-ultramafic complex, Dabieshan UHP terrane, eastern China. *Int Geol Rev* 55(10):1239–1260
- Chen Y, Ye K, Wu YW, Guo S, Su B, Liu JB (2013b) Hydration and dehydration in the lower margin of a cold mantle wedge: implications for crust-mantle interactions and petrogeneses of arc magmas. *Int Geol Rev* 55(12):1506–1522
- Cheng CH, Zhang FR, Yu Q, Lou FS (2010) LA-ICP-MS zircon U-Pb dating of volcanic rocks from Dahajunshan Formation, Wusun Mountians in West Tianshan. *Xinjiang Geol* 27(3):231–235 (in Chinese with English abstract)
- DaPaolo DJ, Daley EE (2000) Neodymium isotopes in basalts of the southwest basin and range and lithospheric thinning during continental extension. *Chem Geol* 169:157–185
- Dong LH, Zhu ZX, Qu X, Wang KZ, Zhao TY (2010) Spatial distribution, geological features and latest research progress of the main ophiolite zones in Xinjiang, NW-China. *Acta Petrol Sin* 26(10):2894–2904 (in Chinese with English abstract)
- Duan SG, Zhang ZH, Jiang ZS, Zhao J, Zhang YP, Li FM, Tian JQ (2014) Geology, geochemistry, and geochronology of the Dunde iron-zinc ore deposit in western Tianshan, China. *Ore Geol Rev* 57:441–461
- Gao J, Klemd R (2003) Formation of HP-LT rocks and their tectonic implications in the western Tianshan Orogen, NW China: geochemical and age constraints. *Lithos* 66:1–22
- Gao J, He GQ, Li MS (1997) Paleozoic orogenic processes of Western Tianshan Orogen. *Earth Sci* 22(1):27–32 (in Chinese with English abstract)
- Gao J, Long LL, Qian Q, Huang DZ, Su W, Klemd R (2006) South Tianshan: a late Paleozoic or a Triassic Orogen. *Acta Petrol Sin* 22(5):1049–1061 (in Chinese with English abstract)
- Gao J, Long LL, Klemd R, Qian Q, Liu DY, Xiong XM, Su W, Liu W, Wang YT, Yang FQ (2009) Tectonic evolution of the South Tianshan orogen and adjacent regions, NW China: geochemical and age constraints of granitoid rocks. *Int J Earth Sci (Geol Rundsch)* 98:1221–1238
- Han BF, Wang S, Jahn BM, Hong DW, Kagami H, Sun Y (1997) Depleted-mantle magma source for the Ulungur River A-type granites from North Xinjiang, China: geochemistry and Nd-Sr isotopic evidence, and implication for Phanerozoic crustal growth. *Chem Geol* 138:135–159
- Han BF, Wang SG, Sun YL, Hong DW (1998) Metaluminous peraluminous granite with positive $\epsilon_{\text{Nd}}(t)$: Yebushan rock from Xinjiang. *Chin Sci Bull* 43(12):1323–1328 (in Chinese)
- Han BF, Guo ZJ, He GQ (2010) Timing of major suture zones in North Xinjiang, China: constraints from stitching plutons. *Acta Petrol Sin* 26(8):2233–2246 (in Chinese with English abstract)
- Han BF, He GQ, Wang XC, Guo ZJ (2011) Late Carboniferous collision between the Tarim and Kazakhstan-Yili terranes in the western segment of the South Tian Shan Orogen, Central Asia, and implications for the Northern Xinjiang, western China. *Earth Sci Rev* 109:74–93
- Hart SR (1984) A large scale isotope anomaly in the Southern Hemisphere mantle. *Nature* 309:753–757
- He GQ, Li MS, Han BF (2001) Geotectonic research of southwest Tianshan and its west adjacent area, China. *Xinjiang Geol* 19(1):7–11 (in Chinese with English abstract)
- Heinhorst J, Lehmann B, Ermolov P, Serykh V, Zhurutin S (2000) Paleozoic crustal growth and metallogeny of Central Asia: evidence from magmatic-hydrothermal ore systems of Central Kazakhstan. *Tectonophysics* 328:69–87
- Hong D, Wang S, Xie X, Zhang J, Wang T (2003) Granitoids and related metallogeny of the Central Asian Orogenic belt. In: Mao J, Goldfarb RJ, Seltman R, Wang D, Xiao W, Hart C (eds) Tectonic evolution and metallogeny of the Chinese Altay and Tianshan. Proceedings volume of the international symposium of the IGCP-473 project in Urumqi and guidebook of the field excursion in Xinjiang, China, 9–21 August 2003. IAGOD Guidebook Series 10: CERCAMS/NHM London, pp 75–106
- Huang BC, John Piper DA, Wang YC, He HY, Zhu RX (2005) Paleomagnetic and geochronological constraints on the post-collisional northward convergence of the southwest Tian Shan, NW China. *Tectonophysics* 409(1–4):107–124
- Jiang CY, Wu WK, Xie GC (1993) Characteristics of Carboniferous volcanic rocks and the trench-arc basin system in the northern part of West Tianshan Mountains. *Acta Petrol et Mineral* 12(3):2–31 (in Chinese with English abstract)
- Jiang CY, Wu WK, Zhang XR, Cui SS (1995) The change from island arc to rift valley—evidence from volcanic rocks in Awulale Area. *Acta Petrol et Mineral* 14(4):289–300 (in Chinese with English abstract)
- Jiang T, Gao J, Klemd R, Qian Q, Zhang X, Xiong XM, Wang XS, Tan Z, Chen BX (2014) Paleozoic ophiolitic mélanges from the South Tianshan Orogen, NW China: Geological, geochemical and geochronological implications for the geodynamic setting. *Tectonophysics* 612–613:106–127
- Jin Z (2010) Chronology and geochemistry of the volcanic rocks of Yuzan Formation in the northern margin of Yili block, Xinjiang Uygur autonomous region. A dissertation submitted for the degree of master, Chang'an university, Xi'an, China (in Chinese with English abstract)
- Klemd R, Gao J, Li JL, Meyer M (2015) Metamorphic evolution of (ultra)-high-pressure subduction-related transient crust in the South Tianshan Orogen (Central Asian Orogenic Belt): Geodynamic implications. *Gondwana Res* 28(1):1–25
- Li ZC (2005) Carboniferous Dahalajunshan Formation volcanic rocks and its mineralized research about Lasitai Region, Kuoerku, Xinyuan. Chang'an University master's degree thesis 1–72 (in Chinese with English abstract)
- Li ZC, Li YJ, Li JH, Luan XD, Guo WJ (2006) Geochemical characteristics of the Dahalajunshan Formation volcanic rocks and their implications on the tectonic setting in Awulale Area. *Xinjiang Geology* 24(2):120–124 (in Chinese with English abstract)
- Li DP (2012) Superimposition mineralization of the Awulale iron deposit belt in western Tianshan, Xinjiang. A Dissertation

- Submitted to China University of Geosciences for Doctoral Degree
- Li JL, Sun S, Hao J, Chen HH, Hou QL, Xiao WJ, Wu JM (1999) Time limit of collision event of collision orogens. *Acta Petrol Sin* 15(2):315–320 (**in Chinese with English abstract**)
- Li YJ, Zhan TJ, Luan XD, Wang XG, Yang GX, Tong LM (2008) Clarification of late Paleozoic unconformities in the Tekes Daban area of West Tianshan and its geological significance. *Acta Geoscientica Sin* 29(2):145–153 (**in Chinese with English abstract**)
- Li YJ, Yang GX, Zhao Y, Luo JC, Zheng DM, Liu YL (2009a) Tectonic framework and evolution of South Tiansharn, NW China. *Geotecton et Metallog* 33(1):94–104 (**in Chinese with English abstract**)
- Li YJ, Li ZC, Zhou JB, Gao ZH, Gao YL, Tong LM, Liu J (2009b) Division of the Carboniferous lithostratigraphic units in Awulale area, western Tianshan. *Acta Petrol Sin* 25(6):1332–1340 (**in Chinese with English abstract**)
- Li JL, Qian Q, Gao J, Su W, Zhang X, Liu X, Jiang T (2010a) Geochemistry, zircon U-Pb Ages and tectonic settings of the Dahalajunshan volcanics and granitic intrusions from the Adengtao Area in the Southeast Zhaosu, Western Tianshan Mountains. *Acta Petrol Sin* 26(10):2913–2924 (**in Chinese with English abstract**)
- Li YJ, Li ZC, Tong LL, Gao ZH, Tong LM (2010b) Revisit the constraints on the closure of the Tianshan ancient oceanic basin: new evidence from Yining block of the Carboniferous. *Acta Petrol Sin* 26(10):2905–2912 (**in Chinese with English abstract**)
- Li T, Xu XY, Li ZP (2011) LA-ICP-MS zircon U-Pb age and geological significance of the Carboniferous Dahalajunshan Group of the Xinyuan County, Xinjiang. *Mineral rock geochemistry Bulletin* 30 (suppl), 66 (**in Chinese**)
- Li YJ, Yang GX, Li H, Jin Z, Ge HY, Lin LQ (2012a) Confirmation of Devonian volcanic rocks from Yining block, Xinjiang and its geological significations. *Acta Petrol Sin* 28(4):1225–1237 (**in Chinese with English abstract**)
- Li T, Xu XY, Li ZP, Bai JK, Ru YJ (2012b) U-Pb zircon geochronology and geochemistry of the volcanic rocks from Dahalajunshan Formation in Kekesu River area, Western Tianshan Mountains. *Geol Bull China* 31(12):1929–1938 (**in Chinese with English abstract**)
- Liu J (2007) Geochemical characteristics and tectonic environment of the Dahalajunshan Formation in Tekesi Daban, Xinjiang. A Dissertation Submitted for the Degree of Master, Chang'an University, 1–73 (**in Chinese with English abstract**)
- Liu B, Chen ZL, Ren R, Han BF, Su L (2013) Timing of the South Tianshan suture zone: New evidence of zircon ages from the granitic plutons in Kokshal area. *Geol Bull China* 32(9):1371–1384
- Liu YM, Yang WH, Gao JY (1994) Study on isotopic age of Dahalajunshan Formation in Tekesi forestry of Xinjiang. *Geochimica* 23(1):99–104 (**in Chinese with English abstract**)
- Long LL, Gao J, Qian Q, Xiong XM, Wang JB, Wang YW, Gao LM (2008) Geochemical characteristics and tectonic settings of Carboniferous volcanic rocks from Yili region, western Tiaoshan. *Acta Petrol Sin* 24(4):699–710 (**in Chinese with English abstract**)
- Luo Y, Niu HC, Shan Q, Zhang B, Zhou CP, Yang WB, Yu XY (2009) Discovery of the basaltic andesite-trachyandesite association in the Yuximolegai Daban, West Tianshan and its geological significance. *Acta Petrol Sin* 25(4):934–943 (**in Chinese with English abstract**)
- Ma YH, Li ZC, Li YJ, Li JH, Luan XD, Guo WJ (2007) Confirming of the Dahalajunshan Formation in the Awulale belt in the western Tianshan. *Gansu Sci Technol* 23(5):94–96 (**in Chinese**)
- Ma XX, Shu LS, Meert JG, Li JY (2014) The Paleozoic evolution of Central Tianshan: Geochemical and geochronological evidence. *Gondwana Res* 25(2):797–819
- MacDonald R, Hawkesworth CJ, Heath E (2000) The Lesser Antilles volcanic chain: a study in arc magmatism. *Earth Sci Rev* 49:1–76
- Niu HC, Shan Q, Luo Y, Yang WB, Zhou CP, Liao SP, Yu XY (2010) Geochronological and geochemical studies on quartz diorite in Yuximoicgai Daban, West Tianshan and its tectonic implication. *Acta Petrol Sin* 26(10):2935–2945 (**in Chinese with English abstract**)
- Qian Q, Gao J, Xiong XM, Long LL, Huang DZ (2006) Petrogenesis and tectonic settings of Carboniferous volcanic rocks from north Zhaosu, western Tianshan Mountains: constraints from petrology and geochemistry. *Acta Petrol Sin* 22(5):1307–1323 (**in Chinese with English abstract**)
- Qian Q, Gao J, Klemd R, He GQ, Song B, Liu DY, Xu RH (2009) Early Paleozoic tectonic evolution of the Chinese South Tianshan Orogen: constraints from SHRIMP zircon U-Pb geochronology and geochemistry of basaltic and dioritic rocks from Xiate, NW China. *Int J Earth Sci (Geol Rundsch)* 98:551–569
- Ru YJ, Xu XY, Li ZP, Chen JL, Bai JK, Li T (2012) LA-ICP-MS zircon U-Pb age and tectonic background of the Dahalajunshan Formation volcanic rocks in Wusunshan area, West Tianshan Mountains. *Geol Bull China* 31(1):50–62 (**in Chinese with English abstract**)
- Scheltens M, Zhang LF, Xiao WJ, Zhang JJ (2015) Northward subduction-related orogenesis of the southern Altaiids: Constraints from structural and metamorphic analysis of the HP/UHP accretionary complex in Chinese southwestern Tianshan, NW China. *Geosci Front* 6(2):191–209
- Shao TQ, Shi Y, Jin H, Song Y, Zhu ZX, Wang KZ, Zhang JD, Xu D (2006) Volcanic rock petrochemical characteristics of the Dahalajunshan Formation in the Western Tianshan, Xinjiang and their geological significance. *Xinjiang Geol* 24(3):218–222 (**in Chinese with English abstract**)
- Shu LS, Wang B, Zhu WB (2007) Age of radiolarian fossils from the Heiyingshan ophiolitic mélange, southern Tianshan belt, NW China, and its tectonic significance. *Acta Geol Sin* 81(9):1–8 (**in Chinese with English abstract**)
- Sun LH, Pen TP, Wang YJ (2007) Geological characteristics of basaltic andesites from Dahalajunshan Formation, southeastern Tekesi (Xinjiang): petrogenesis and its tectonic significance. *Geotectonica et Metallog* 31(3):372–379 (**in Chinese with English abstract**)
- Sun JM, Ma ZP, Xu XY, Li XY, Weng K, Zhang T (2012) The formation epoch of the host wall rock of the Beizhan iron deposit in West Tianshan Mountains of Xinjiang and its geological significance. *Geol Bull China* 31(12):1973–1982 (**in Chinese with English abstract**)
- Tang YQ, Gao J, Zhao M, Wang J (1995) The ophiolite and blueschists in the Southwestern Tianshan orogenic belt Xinjiang, Northwestern China. Beijing: Geological Publishing House, 1–133 (**in Chinese**)
- Tang GJ, Wang Q, Wyman AD, Li ZX, Xu YG, Zhao ZH (2012) Metasomatized lithosphere–asthenosphere interaction during slab roll-back: Evidence from Late Carboniferous gabbros in the Luotuogou area, Central Tianshan. *Lithos* 155(12):67–80
- Tang GJ, Wang Q, Wyman AD, Sun M, Zhao ZH, Jiang ZQ (2013) Petrogenesis of gold-mineralized magmatic rocks of the Taerbieke area, northwestern Tianshan (western China): Constraints from geochronology, geochemistry and Sr–Nd–Pb–Hf isotopic compositions. *J Asian Earth Sci* 74:113–128
- Wang BY, Lang ZJ, Li XD, Qu X, Li TF, Huang C, Chui X (1994) Study on the geological sections across the western segment of

- Tianshan Mountains, China. Science Press, Beijing, pp 1–202 (in Chinese)
- Wang B, Shu LS, Cluzel D, Faure M, Charvet J (2007) Geochemical constraints on Carboniferous volcanic rocks of the Yili Block (Xinjiang, NW China): Implication for the tectonic evolution of Western Tianshan. *J Asian Earth Sci* 29:148–159
- Wang B, Cluzel D, Shu LS, Faure M, Charvet J, Chen Y, Meffre S, Jong KD (2009) Evolution of calc-alkaline to alkaline magmatism through Carboniferous convergence to Permian transcurrent tectonics, western Chinese Tianshan. *Int J Earth Sci* 98:1275–1298
- Wang QC, Shu LS, Charvet J, Faure M, Ma HD, Natal'in B, Gao J, Kröner A, Xiao WJ, Li JY, Windley B, Chen Y, Glen R, Jian P, Zhang W, Seltmann R, Wilde S, Choulet F, Wan B, Quinn C, Rojas-Agramonte Y, Shang QH, Zhang W, Wang B, Lin W (2010) Understanding and study perspectives on tectonic evolution and crustal structure of the Paleozoic Chinese Tianshan. *Episodes* 33:242–266
- Wang M, Zhang JJ, Zhang B, Qi GW (2014) An Early Paleozoic collisional event along the northern margin of the Central Tianshan Block: Constraints from geochemistry and geochronology of granitic rocks. *J Asian Earth Sci.* doi:[10.1016/j.jse-aes.2014.07.001](https://doi.org/10.1016/j.jse-aes.2014.07.001). (in press)
- Windley BF, Alexeiev D, Xiao W, Kröner A, Badarch G (2007) Tectonic models for accretion of the Central Asian Orogenic Belt. *J Geol Soc Lond* 164:31–47
- Wu SM, Lu HF, Ma RS, Jia D, Cai DS (1995) Classification of tectonic facies and their evolutionary features in the west Tianshan Mountains. *Reg Geol China* 14(2):149–156 (in Chinese with English abstract)
- Xia LQ, Li XM, Xia ZC, Xu XY, Ma ZP, Wang LS (2006) Carboniferous-Permian rift-related volcanism and mantle plume in the Tianshan, northwestern China. *Northwest Geol* 39(1):1–49 (in Chinese with English abstract)
- Xia LQ, Xia ZC, Xu XY, Li XM, Ma ZP, Wang LS (2007) The discriminate basalt between continental basalt and island arc based on geochemical method. *Acta Petrol et Mineral* 26(1):77–89 (in Chinese with English abstract)
- Xia LQ, Xia ZC, Xu XY, Li XM, Ma ZP (2008) Relative contributions of crust and mantle to the generation of the Tianshan Carboniferous rift-related basic lavas, northwestern China. *J Asian Earth Sci* 31(4–6):357–378
- Xia H, Chen GW, Liu Q, Luo Y (2011) Geochemical characteristics of the Dahalajunshan formation volcanic rocks in the Tulasu Basin of Western Tianshan and its tectonic implications. *Geotecton et Metallog* 35(3):429–438 (in Chinese with English abstract)
- Xia LQ, Xu XY, Li XM, Ma ZP, Xia ZC (2012) Reassessment of petrogenesis of Carboniferous-Early Permian rift-related volcanic rocks in the Chinese Tianshan and its neighboring areas. *Geosci Front* 3(4):445–471
- Xiao WJ, Santosh M (2014) The western Central Asian Orogenic Belt: a window to accretionary orogenesis and continental growth. *Gondwana Res* 25:1429–1444
- Xiao XC, Liu X, Gao R (2004a) The crustal structure and tectonic evolution of southern Xinjiang. Commercial Press, Beijing, pp 1–270 (in Chinese with English abstract)
- Xiao WJ, Windley BF, Badarch G, Sun S, Li J, Qin K, Wang ZH (2004b) Paleozoic accretionary and convergent tectonics of the southern Altaiids: implications for the Lateral growth of Central Asia. *Journal of the Geological Society. London* 161:339–342
- Xiao L, Hayward N, Begg G, Fu ML, Wang FZ, Pirajno F (2005) The Jinxi-Yelman high-sulfidation epithermal gold deposit, Western Tianshan, Xinjiang Province, P. R. China. *Ore Geol Rev* 26(1–2):17–37
- Xiao WJ, Windley BF, Allen MB, Han CM (2013) Paleozoic multiple accretionary and collisional tectonics of the Chinese Tianshan orogenic collage. *Gondwana Res* 23:1316–1341
- Xu XY, Xia LQ, Ma ZP, Wang YB, Xia ZC, Li XM, Wang LS (2006) SHRIMP zircon U-Pb geochronology of the plagiogranites from Bayingou ophiolite in North Tianshan Mountains and the petrogenesis of the ophiolite. *Acta Petrol Sin* 22(1):83–94 (in Chinese with English abstract)
- Xu XY, Wang HL, Li P, Chen JL, Ma ZP, Zhu T, Wang N, Dong YP (2013) Geochemistry and geochronology of Paleozoic intrusions in the Nalati (Narati) area in western Tianshan, Xinjiang, China: implications for Paleozoic tectonic evolution. *J Asian Earth Sci* 72:33–62
- Yang JZ, Zhao YL, Wang YJ, Jiang XW (2003) Sedimentary environment and mineralization of Dahalajunshan Formation in west Tianshan orogenic belt, Xinjiang. *Geol Prospect* 39(2):1–5 (in Chinese with English abstract)
- Yang GX, Li YJ, Guo WJ, Bi MB, Luan XD, Li ZC, Li H, Tong LM (2008) Petrochemical evidence and its significance of disintegration of Kuorku Granite Batholith in Awulale, Western Tianshan. *J Earth Sci Environ* 30(2):125–129, 155 (in Chinese with English abstract)
- Yang FQ, Mao JW, Bierlein FP, Pirajno F, Zhao CS, Ye HS, Liu F (2009) A review of the geological characteristics and geodynamic mechanisms of Late Paleozoic epithermal gold deposits in North Xinjiang, China. *Ore Geol Rev* 35:217–234
- Yang WB, Niu HC, Shan Q, Luo Y, Sun WD, Li CY, Li NB, Yu XY (2012) Late Paleozoic calc-alkaline to shoshonitic magmatism and its geodynamic implications, Yuximolegai area, western Tianshan, Xinjiang. *Gondwana Res* 22(1):325–340
- Zhai W, Sun XM, Gao J, He XP, Liang JL, Miao LC, Wu YL (2006) SHRIMP dating of zircons from volcanic host rocks of Dahalajunshan Formation in Axi gold deposit, Xinjiang, China, and its geological implications. *Acta Petrol Sin* 22(5):1399–1404 (in Chinese with English abstract)
- Zhai W, Sun XM, Sun WD, Su LW, He XP, Wu YL (2009) Geology, geochemistry, and genesis of Axi: a Paleozoic low-sulfidation type epithermal gold deposit in Xinjiang, China. *Ore Geol Rev* 36(4):265–281
- Zhang JD (2012) Some understandings about Carboniferous Strata and Biota of Western Tianshan, Xinjiang. *Xinjiang Geol* 30(z1):38–44 (in Chinese with English abstract)
- Zhang JS, Li CZ, (2006) Tectonic Setting of the Dahalajunshan Formation Volcanic Rocks in Awulale of West Tianshan. *Gansu Geology* 15(2):10–14 (in Chinese with English abstract)
- Zhang LF, Ellis DJ, Arculus RJ, Jiang W, Wei C (2003) ‘Forbidden zone’ subduction of sediments to 150 km depth—the reaction of dolomite to magnesite + aragonite in the UHPM metapelites from western Tianshan, China. *J Metamorph Geol* 21:523–529
- Zhang LF, Ai YL, Li XP, Daniela R, Song B, Samantha W, Song SG, David E, Liou JG (2007) Triassic collision of western Tianshan orogenic belt, China: Evidence from SHRIMP U-Pb dating of zircon from HP/UHP eclogitic rocks. *Lithos* 96(1–2):266–280
- Zhang FR, Chen CH, Yu Q, Lou FS (2009) LA-ICP-MS zircon U-Pb dating of volcanic rocks from Dahalajunshan formation, Wusun Mountains in west Tianshan, Xinjiang. *Geol Geol* 27(3):231–235 (in Chinese with English abstract)
- Zhao XB, Xue CJ, Symons DTA, Zhang ZC, Wang HG (2014) Microgranular enclaves in island-arc andesites: A possible link between known epithermal Au and potential porphyry Cu-Au deposits in the Tulasu ore cluster, western Tianshan, Xinjiang, China. *J of Asian Earth Sci* 85:210–223
- Zhou X, Yu XQ, Wang ZX, Xiao WF, Li CL, Li PJ, Tong JC (2015) SHRIMP U-Pb zircon geochronological and geochemical data of the Early Carboniferous Dahalajunshan Formation: evidence for the subduction processes in western Tianshan. *Geol Bull China* 34(5):845–860

- Zhu YF, Ogasawara Y, (2002a) Carbon recycled into deep Earth: evidence from dolomite dissociation in subduction-zone rocks. *Geol* 30:947–950
- Zhu YF, Ogasawara Y, (2002b) Phlogopite and coesite exsolution from super-silicic clinopyroxene. *Int Geol Rev* 44:831–836
- Zhu YF, Ogasawara Y, (2004) Clinopyroxene phenocrysts (with green euhedral cores) in Irachybasalts: implications for two magma chambers under the Kokchetav UHP massif, North Kazakhstan. *J Earth Asian Sci* 22:517–527
- Zhu YF, Zhang LF, Gu LB, Guo X, Zhou J (2005a) The zircon SHRIMP chronology and trace element geochemistry of the Carboniferous volcanic rocks in western Tianshan Mountains. *Chin Sci Bull* 50(19):2201–2212 (**in Chinese with English abstract**)
- Zhu YF, Zhou J, Zhang LF (2005b) The zircon SHRIMP chronology of the Dahalajunshan Formation in West Tianshan, Xinjiang. *Abstracts of Petrology and Geodynamics Meeting*. Hangzhou, China, 424–425 (**in Chinese**)
- Zhu YF, Zhang LF, Gu LB, Guo X, Zhou J (2006a) Age of the “Dahalajunshan” Formation in Xinjiang and its disintegration. *Geol China* 33(3):487–497 (**in Chinese with English abstract**)
- Zhu YF, Zhou J, Guo X (2006b) Petrology and Sr-Nd isotopic geochemistry of the Carboniferous volcanic rocks in the western Tianshan Mountains, NW China. *Acta Petrol Sin* 22(5):1341–1350 (**in Chinese with English abstract**)
- Zhu YF, Guo X, Song B, Zhang LF, Gu LB (2009) Petrology, Sr-Nd-Hf isotopic geochemistry and zircon chronology of the Late Palaeozoic volcanic rocks in the south western Tianshan Mountains, Xinjiang, NW China. *J Geol Soc* 166:1085–1099
- Zhu YF, An F, Xue YX, Chen B, Zhang LF (2010) Zircon U-Pb age for Kesang Rondong volcanic rocks, Southwest Tianshan Mts., Tekes, Xinjiang. *Acta Petrol Sin* 26(8):2255–2263 (**in Chinese with English abstract**)
- Zhu ZX, Li J, Dong LH, Wang KZ, Zhang XF, Xu SQ (2011) Geological characteristics and tectonic significance of Paleozoic intrusive rocks in Western Tianshan of Xinjiang Uygur Autonomous Region. *Earth Sci Front* 18(2):170–179 (**in Chinese with English abstract**)
- Zhu ZX, Dong LH, Liu SC, Li JY, Wang KZ, Zhao TY, Li P, Jin LY (2012) Volcanic rock geological characteristics and tectonic significance of the late Paleozoic Yili Block in the Western Tianshan, Xinjiang. *Xinjiang Geol* 30(3):258–263 (**in Chinese with English abstract**)